

UC Irvine

UC Irvine Electronic Theses and Dissertations

Title

Improving the Blade Coating Method for PEMFC Catalyst Coated Membrane Fabrication

Permalink

<https://escholarship.org/uc/item/8f49t9q3>

Author

Sun, Shikai

Publication Date

2024

Peer reviewed|Thesis/dissertation

UNIVERSITY OF CALIFORNIA,
IRVINE

Improving the Blade Coating Method for PEMFC Catalyst Coated Membrane Fabrication

THESIS

submitted in partial satisfaction of the requirements
for the degree of

MASTER OF SCIENCE

in Materials Science and Engineering

by

Shikai Sun

Thesis Committee:
Associate Professor Iryna Zenyuk, Chair
Professor Plamen Atanassov
Professor Jacob Brouwer

2024

DEDICATION

To

my families and friends

in recognition of their support and help

TABLE OF CONTENTS

LIST OF FIGURES.....	iv
LIST OF TABLES.....	viii
ACKNOWLEDGEMENTS	ix
ABSTRACT OF THE THESIS.....	x
INTRODUCTION.....	1
CHAPTER 1: Background.....	3
1.1 Proton-Exchange Membrane Fuel Cells.....	3
1.1.1 Membrane Electrode Assembly.....	4
1.1.2 Flow Field and Sealing Gaskets.....	6
1.2 Catalyst Coated Membrane Fabrication.....	7
1.2.1 Air-spraying Method.....	7
1.2.2 Decal Transfer Method.....	9
1.2.3 Blade Coating Method.....	11
CHAPTER 2: Experimental.....	14
2.1 Equipment and Materials.....	14
2.1.1 Materials for CCM Fabrication.....	14
2.1.2 Electrochemical Characterization.....	14
2.2 Catalyst Ink.....	15
2.2.1 Composition.....	15
2.2.2 Fabrication.....	17
2.3 Procedure of Blade Coating.....	18
2.4 Electrochemical Characterization.....	19
2.5 Analysis of Electrochemical Data.....	21
CHAPTER 3: Results and Discussion.....	25
3.1 Nafion MEA.....	25
3.1.1 Ink Configuration and Coating Effects.....	25
3.1.2 Electrochemical Characterization.....	33
3.2 Pemion MEA.....	35
3.3 Limiting Current Test.....	38
3.4 BCM with Other Materials.....	39
SUMMARY AND CONCLUSIONS.....	41
REFERENCE.....	42

LIST OF FIGURES

Figure 1.1. A schematic drawing of a PEMFC.....	3
Figure 1.2. (a) Structure of Nafion; (b) Structure of Pemion. In Nafion structure, PTFE component provides material stability and maintains low breathability, while the PFSA component provides high ionic conductivity. Pemion is a hydrocarbon-based ionomer, which did not contain fluorinated structure.....	5
Figure 1.3. (a) 25 cm ² serpentine channel flow field; (b) FR-PTFE sealing gasket with GDL. Different flow field designs have different advantages. Larger flow channels can deliver gas and water more efficiently, but can cause uneven compression of the GDL and increase contact resistance. The thickness of gasket can control the compression percent of GDL, which can significantly affect the contact resistances between CL-GDL-flow field.....	6
Figure 1.4. Schematic diagram of Air Spraying Method. The spray pattern shape (1st run path in red, 2nd run path in black) and height of the nozzle can significantly affect coating effects.....	8
Figure 1.5. Schematic diagram of Decal Transfer Method. The coating process includes a) catalyst ink fabrication; b) doctor blade coating on PTFE substrate; c) decal drying; d) hot pressing to transfer decal to PEM.....	9
Figure 1.6. Schematic diagram of Blade Coating Method. a) equipment setup; b) blade coating illustration; c) coating effect. The coating area on the PEM was limited by the window on Kapton mask.....	11
Figure 2.1. Coating effect with different ink viscosity. a) ink with low viscosity resulted in part of the area that was not coated; b) ink with high viscosity resulted in different parts have	

different drying speeds resulting in coffee-ring effects; c) ink with very high viscosity resulted in a very strong coffee-ring effect leading to the catalyst layer being shattered..... 17

Figure 2.2. Integral area (gray) for a) HUPD and b) CO stripping when calculating ECSA..... 22

Figure 3.1. a) CCM made by BCM with 0.95 mgPt/cm²; b) polarization curve and HFR data; c) comparison of HFR-corrected polarization curve of BCM-prepared CCM and an ASM-prepared benchmark CCM with 0.378 mgPt/cm² catalyst loading on cathode; d) comparison of HFR-corrected current density at 0.7V. Under this high catalyst loading, good CCM can be easily fabricated by BCM..... 26

Figure 3.2. a) CCM made by BCM with 0.28 mgPt/cm²; b) polarization curve and HFR data; c) comparison of HFR-corrected polarization curve of BCM-prepared CCM and an ASM-prepared benchmark CCM with 0.378 mgPt/cm² catalyst loading on cathode; d) comparison of ECSA and HFR-corrected current density. For this CCM, the ECSA was fine, but the activation loss was significantly higher than ASM-prepared CCM..... 27

Figure 3.3. Catalyst loading for each attempt in Table 3.1. The target loading is 0.3 mgPt/cm², and this can be reached (±10%) by BCM runs on 60°C vacuum plate, using ink with 17.38 mgPt/mL to coat for 4 passes with 50uL each time..... 28

Figure 3.4. a) CCM made by BCM with 0.24 mgPt/cm²; b) LSV data for this CCM. Significant elongation was found when doing BCM. The LSV curve shows a noticeable slope, which proved the structure of CCM has being damaged by applying ink repeatedly and generously to the PEM..... 29

Figure 3.5. Catalyst loading on CCMs using the same ink, but with different coating temperatures. The slope of 80°C BCM is close to two times that of the 60°C BCM. This shows that a lower coating temperature can reduce the catalyst loading by using the same ink..... 30

Figure 3.6. a) CCM made by BCM with 0.26 mgPt/cm²; b) polarization curve and HFR data; c) comparison of HFR-corrected polarization curve of BCM-prepared CCM and an ASM-prepared benchmark CCM with 0.378 mgPt/cm² catalyst loading on cathode; d) comparison of ECSA and HFR-corrected current density. CCM coated on 60°C vacuum table, with catalyst ink using 1:1:0.1 water:IPA:EG. This CCM shows good ECSA and cell performance, and is the Nafion benchmark for BCM..... 34

Figure 3.7. Comparison of a) polarization curve and HFR data; b) HFR corrected polarization curve between BOL and after four times voltage recovery. Note that at high current density for BOL, there is a significant rise in HFR. This can be caused by the existence of EG residual. After recovery cycles, the EG residual was removed, so that the high current density rise in HFR disappeared..... 35

Figure 3.8. Pemion CCM coated by catalyst ink with a solvent ratio of water:IPA:EG a) 1:1:0.3; b) 1:1:0.1; c) 1:1:0.05. Note that coffee-ring effects were found on all of these three CCM. For 1:1:0.3, the CL was shattered by coffee-ring effect during drying. For 1:1:0.05, the effect is acceptable, but for future CCM, an even lower EG ratio should be used..... 36

Figure 3.9. a) CCM made by BCM with 0.21 mgPt/cm²; b) polarization curve and HFR data; c) HFR-corrected polarization curve of BCM/ASM-prepared CCM, the current density at 0.7V for BCM is 0.8 A/cm²; d) comparison of ECSA and HFR-corrected current density. CCM coated on 60°C vacuum table, with catalyst ink using 1:1:0.05 water:IPA:EG. This CCM shows good

ECSA and cell performance, but it is noticeable that the mass transport loss is higher than the ASM-prepared CCM..... 37

Figure 3.10. Oxygen transport resistance tested under different backpressure and scanning speed.

a) plotting of backpressure vs. R_t , which is calculated in equation 2.2; b) calculated OTR under different condition. The bar plot shows that the OTR would decrease as RH increase, while scanning rate would not have significant influence to the OTR..... 39

LIST OF TABLES

Table 3.1. Attempts to reach target cathode catalyst loading 0.3 mgPt/mL.....	27
Table 3.2. Attempts to achieve different solvent ratios. The images on the fourth column show a trend of the single pass BCM coating dependence upon viscosity. When viscosity goes lower, a larger part of PEM will not be coated after blade runs by. When viscosity goes higher, a stronger coffee-ring effect will happen.....	30

ACKNOWLEDGEMENTS

I would like to express my deepest appreciation to Professor Iryna Zenyuk, my thesis advisor and the committee chair, for giving me the opportunity to explore the field of proton exchange membrane fuel cells. Professor Zenyuk's guidance has been instrumental in steering my research direction. I also wish to thank Professor Plamen Atanassov and Professor Jacob Brouwer for being part of my thesis committee.

During my two years study in the Iryna group, I received valuable advice from my colleagues. I am grateful to Chief Scientist Dr. Yu Morimoto for his encouragement and support of my research. It has been an honor to collaborate with Robert Anton and Dr. Bilal Iskandarani. Thanks to Dr. Ziliang Gao for his patient guidance when I first joined the Iryna group. Thanks to Thirawit Sornsuchat for his encouragement over these two years. Lastly, I appreciate the National Fuel Cell Research Center for providing me with an excellent experimental environment.

I would like to deeply gratitude to the Plug Power for funding this research.

ABSTRACT OF THE THESIS

Improving the Blade Coating Method for PEMFC Catalyst Coated Membrane Fabrication

by

Shikai Sun

Master of Science in Materials Science and Engineering

University of California, Irvine, 2024

Associate Professor Iryna Zenyuk, Chair

In recent years, the global energy demand continues rising, and the extensive usage of fossil fuels have caused severe environmental problems. As an efficient and clean electrochemical energy conversion device, Proton Exchange Membrane Fuel Cell (PEMFC) have attracted more and more attentions.

The catalyst-coated membrane (CCM) is crucial to PEMFCs, directly impacting their performance and durability. This study evaluated traditional CCM manufacturing methods, such as air spraying and decal transfer, and identified their limitations in material efficiency or scalability. Compare to these two methods, the blade coating method (BCM) has the ability to precisely control the thickness and uniformity of the catalyst layer, and is friendly for scale production due to high material efficiency and reproducibility. However, existing blade coating methods struggle to produce uniform catalyst layers at lower target catalyst loadings for hydrocarbon ionomer Pemion™. This study introduced ethylene glycol into the solvent system to adjust the viscosity of the catalyst ink to solve this issue. By experimentally investigating the composition of the catalyst ink and the operational parameters during coating, we successfully prepared a CCM with a cathode catalyst loading of 0.3 mgPt/cm² using BCM, achieving good

uniformity in the catalyst layer while the MEA's performance approached that of CCMs prepared using ASM (0.8 A/cm^2 at 0.7 V).

The improved blade coating process significantly enhances the uniformity of the catalyst layer. By using the improving process, BCM can achieve comparable performance to traditional CCM manufacturing methods. Given its high repeatability, fast speed, and ease of scaling up, researching, developing, and improving BCM could contribute to technological advancements in PEMFCs and the practical application.

INTRODUCTION

As the climate change and resource depletion problems become more and more serious, many countries around the world are turning to renewable energy sources, such as wind and solar power, to reduce their reliance on fossil fuels [1]. However, the development of these energy sources brings complications such as energy curtailment, where excess energy is often wasted [2,3]. Significant energy curtailments have been documented in California, because of the mismatch between solar production during the day and peak energy demand at night [4].

Hydrogen can be used as a compelling solution to relieve the curtailment problems. As an energy carrier, hydrogen can store excess renewable energy through the electrolyzer [5]. The stored hydrogen can be converted back into electricity during peak demand periods, or directly used in transport or industrial processes by hydrogen fuel cells. Additionally, by injecting in existing natural gas pipelines, hydrogen can be transported and stored for long periods of time, providing a buffer and increasing the flexibility and resiliency of the energy system [6]. To rapidly develop hydrogen energy-related infrastructure and economy, the U.S. Department of Energy launches the “Hydrogen Shot” program [7]. The program aims to cut the cost of clean hydrogen production to \$1 per kilogram within a decade, making it an economically viable option for large-scale deployment. The shift to a hydrogen economy not only supports decarbonization efforts, but also boosts economic growth by creating new markets and industries in sustainable technologies field.

While solving the renewable energy storage problem through hydrogen production is important, developing green electrochemical conversion devices is equally important. The widespread use of fossil fuels among the world, especially in transportation, results in significant greenhouse gas emissions [8]. In order to reduce the dependence on fossil fuels, research on

proton exchange membrane fuel cells (PEMFC) has received attention in recent years. Major automakers, such as Toyota and Hyundai have developed and commercialized PEMFC-powered light vehicles. Using hydrogen as a fuel allows for longer ranges at a lighter weight due to its high net energy density [9]. Therefore, PEMFCs using hydrogen as fuel are considered to be an excellent choice for powering clean energy vehicles.

As an important part of PEMFC, the preparation of catalyst layer has always been a hot topic of research. Compared with the air spray method (ASM), the blade coating method (BCM) can precisely control the thickness and uniformity of the catalyst layer as decal transfer method (DTM), but don't need to apply hot pressing [10], so BCM would be applicable to those ionomers have high glass transition temperature, like PemionTM ($T_g \approx 300^\circ\text{C}$.) Furthermore, due to its higher material efficiency and fewer steps, BCM can be easily scaled to larger production volumes, which is beneficial for industrial applications.

CHAPTER 1: Background

1.1 Proton-Exchange Membrane Fuel Cells

Polymer electrolyte membrane fuel cell (PEMFC) is an electrochemical device that can convert chemical energy stored in hydrogen into electrical energy and thermal energy. The components of PEMFC include membrane electrode assembly (MEA), sealing gasket, and flow field [11]. Hydrogen is delivered to the anode through the flow field, while air is delivered to the cathode. Between the flow fields, a proton exchange membrane (PEM) is coated with catalyst layers on both sides, and being sandwiched by two gas diffusion layers (GDL).

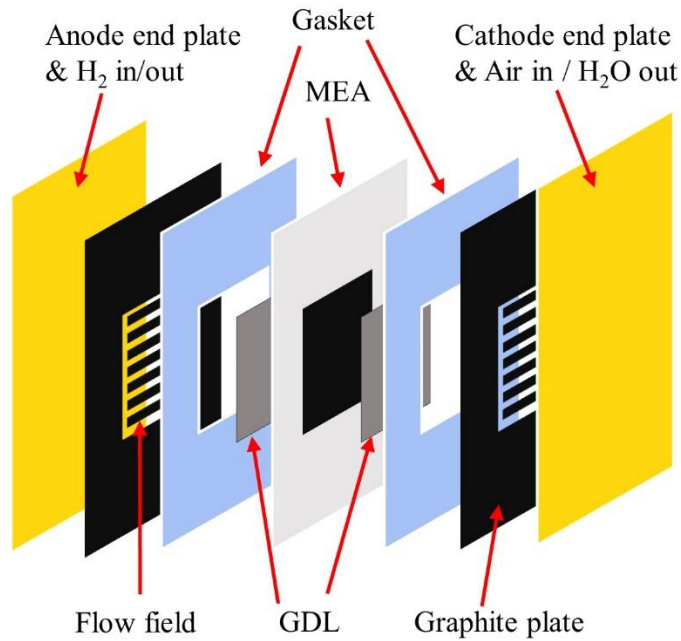
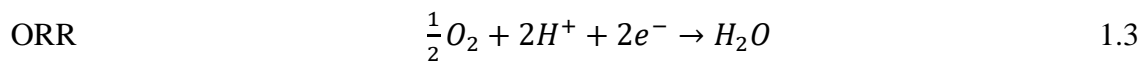
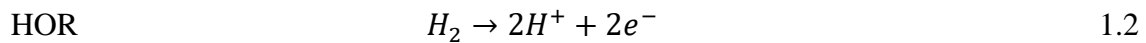
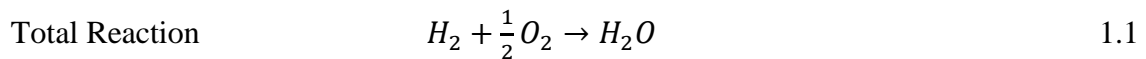


Figure 1.1. A schematic drawing of a PEMFC.



Electrochemical reactions (Reaction 1.1) occur on platinum nanoparticles within this catalyst layer. Hydrogen oxidation reaction (Reaction 1.2) occurs at the anodes, oxidizing the supplied hydrogen into protons (H^+) and electrons. A proton exchange membrane allows protons to pass through the membrane to the cathode, while electrons must follow an external circuit to reach the cathode. The oxygen reduction reaction (Reaction 1.3) occurs at the cathode, where oxygen combines with protons and electrons to form water and heat. This process produces an electric current flowing through the external circuit, with water being the only by-product [13]. Therefore, PEMFC is a pollution-free electrochemical energy conversion equipment.

1.1.1 Membrane Electrode Assembly

The membrane electrode assembly (MEA) is the key component of the proton exchange membrane fuel cell (PEMFC), where proton transport and electrode reactions occur [12]. MEA usually being assembled by three parts: proton exchange membrane (PEM), catalyst layer (CL) and gas diffusion layer (GDL). The layers of MEA are arranged in order from anode to cathode: anode GDL, anode CL, PEM, cathode CL, cathode GDL [14].

PEMs are usually formed by ionomers. Currently, PEM in commercial applications mainly uses *Nafion* (Figure 1.2a) as the ionomer. *Nafion* is made up of polytetrafluoroethylene (PTFE) backbone and perfluorosulfonic acid (PFSA) side chains. The PTFE component provides material stability and maintains low breathability, while the PFSA component provides high ionic conductivity [15]. Since fluorinated compounds may cause harm to the environment after degradation, and the potential bans of PFAS by European Union in 2030 [16], research on hydrocarbon-based ionomers *Pemion* (Figure 1.2b) is also a focus [17].

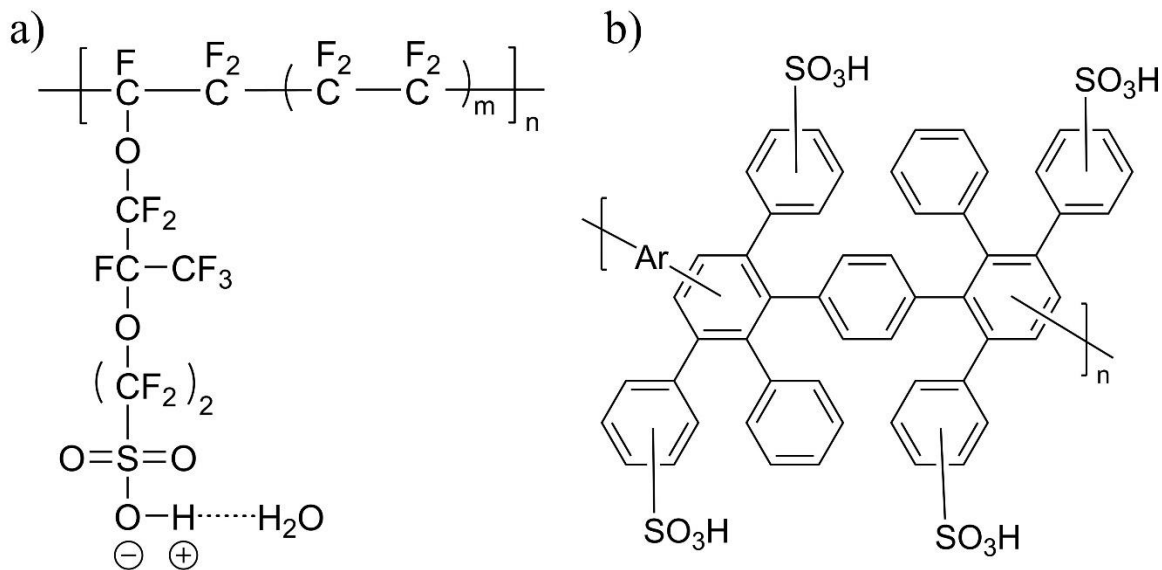


Figure 1.2. (a) Structure of *Nafion*; (b) Structure of *Pemion*. In *Nafion* structure, PTFE component provides material stability and maintains low breathability, while the PFSA component provides high ionic conductivity. *Pemion* is a hydrocarbon-based ionomer, which did not contain fluorinated structure.

In order to reach high porosity, catalyst layers (CL) are usually formed attached to the PEM or GDL. These two CL fabrication methods are commonly referred to as the catalyst-coated membrane (CCM) method and the gas diffusion electrode (GDE) method. The CCM method usually coating CL directly on PEM, or initially on a polytetrafluoroethylene film and then transferring it to PEM by hot pressing. In contrast, the GDE method usually coating CL onto GDL and then hot press directly with PEM to assemble the MEA.

In PEMFC, gas diffusion layer (GDL, Figure 1.3b) is mainly used to transport the reaction gas into the CL and remove the water produced by the reaction from the CL. The electrons generated at the anode also need to be guided to the flow field through the GDL and then to the

cathode through an external circuit. In addition, GDL conducts the heat generated during the reaction, ensuring that the reaction proceeds at stable temperature and relative humidity [20].

1.1.2 Flow Field and Sealing Gaskets

In PEMFCs, the flow field (Figure 1.3a) is usually composed of conductive materials like graphite. Through multiple parallel serpentine channels, the flow field evenly distributes the gas to the MEA and remove water generated during the electrochemical reaction from the system [14]. Different flow field designs have different advantages. For example, larger flow channels can deliver gas and water more efficiently, but can cause uneven compression of the GDL and increase contact resistance [14]. Since a single PEMFC usually produces a voltage less than 1V, multiple PEMFCs must be stacked in series to obtain the required power in practical applications. The series connection is usually accomplished by separating multiple MEAs with bipolar plates with etched channels on both sides.

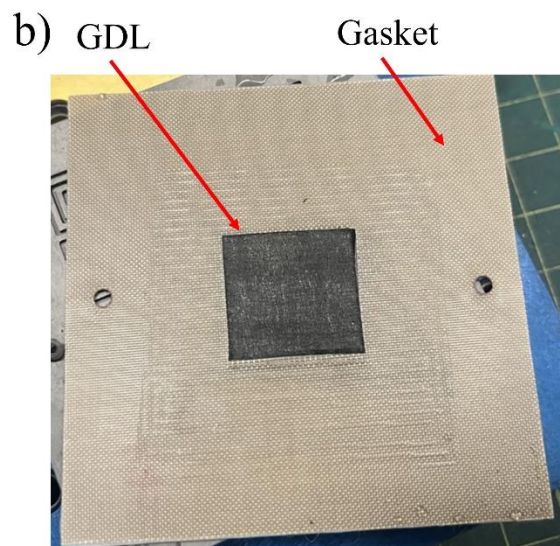
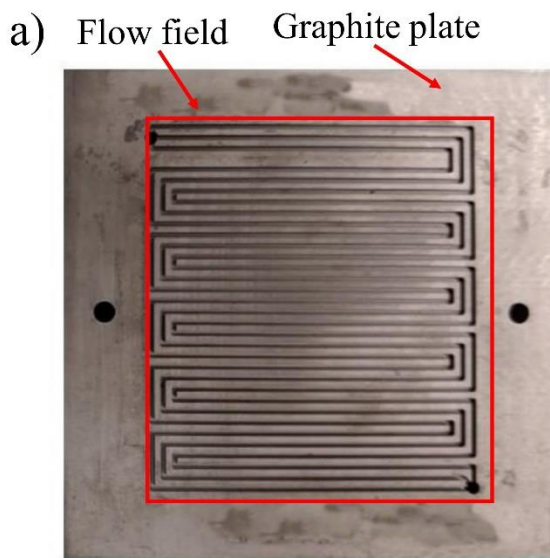


Figure 1.3. (a) 25 cm² serpentine channel flow field; (b) FR-PTFE sealing gasket with GDL. Different flow field designs have different advantages. Larger flow channels can deliver gas and water more efficiently, but can cause uneven compression of the GDL and increase contact resistance. The thickness of gasket can control the compression percent of GDL, which can significantly affect the contact resistances between CL-GDL-flow field.

The sealing gasket is usually located between the flow field and the MEA in the PEMFC, one on each side of the cathode and anode. In a laboratory setting, a gasket (Figure 1.3b) typically has a similar area to the flow field but includes a window the same size as the GDL to allow direct contact of the GDL with the flow field. This design also shields the inactive areas of the membrane and is therefore widely adopted [14]. Gaskets, typically made from a combination of fiber-reinforced polytetrafluoroethylene (FR-PTFE) and standard PTFE of varying thicknesses, are used to seal the PEMFC during flow field compression to prevent gas or liquid leakage. In addition, changing the combination of sealing gasket thickness can control the degree of compression on the GDL. For example, to achieve 20% compression on a GDL with 250 μm thickness, a gasket combination with a total thickness of 200 μm is required. Parkinson et al. [21] finds that GDL compression can significantly affect the contact resistances between CL-GDL-flow field.

1.2 Catalyst Coated Membrane Fabrication

1.2.1 Air-spraying Method

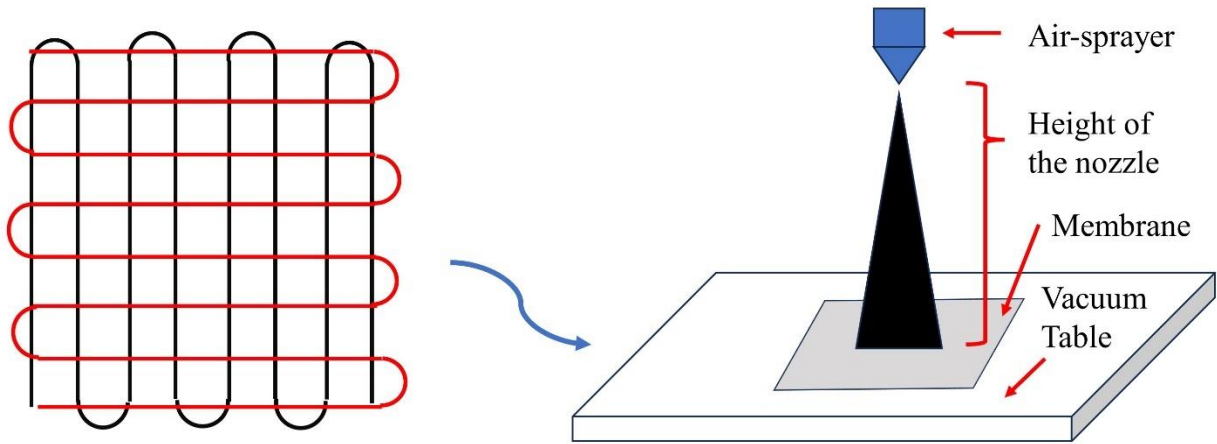


Figure 1.4. Schematic diagram of Air Spraying Method. The spray pattern shape (1st run path in red, 2nd run path in black) and height of the nozzle can significantly affect coating effects.

Air spraying method (ASM) is a method that has been widely used in the fabrication of CCM. This method uses compressed air to atomize the catalyst ink into tiny droplets, which are then sprayed onto the surface of the CCM to form CL. Turtayeva et al. found that by adjusting spraying pressure, distance between nozzle and support, spraying speed and other parameters, a uniform CL and good PEMFC performance can be obtained [23]. Martin et al. [36] compared the microstructures of catalyst layers (CL) obtained through different methods including ultrasonic spraying, air brushing, and electrospraying. The results indicated that due to the absence of an ultrasonic generator at the nozzle head, particles tend to agglomerate during the coating process when using ASM, significantly affecting the uniformity of the CL. Kim et al. [37] examined the effects of using different ionomer to carbon (I/C) ratios in the catalyst ink on the performance of the resulting catalyst-coated membranes (CCM). The findings suggested that the structure of the catalyst layer in ASM applications leads to variations in the ionomer's ionic conductivity, thereby influencing the performance of the membrane electrode assembly (MEA). Deschamps et al. [38] tested two different spraying configurations with varying distances and characterized the surface morphology of the samples using contact profilometry and 3D laser scanning

microscopy. The results demonstrated that the topological structure of the deposited layers varied with the different spraying configurations. In terms of catalyst ink formulations, ASM usually uses compositions with lower viscosity and catalyst concentration to achieve better ink atomization. Spraying is usually carried out on a heating plate, which quickly evaporates the IPA in the solvent by heating, avoiding damaging the structure of the PEM. By using related machinery for spraying (Figure 1.4), this method has the advantages of high reproducibility and less catalyst waste, but it also has the disadvantages of slow speed and inconvenient rapid expansion of production scale.

1.2.2 Decal Transfer Method

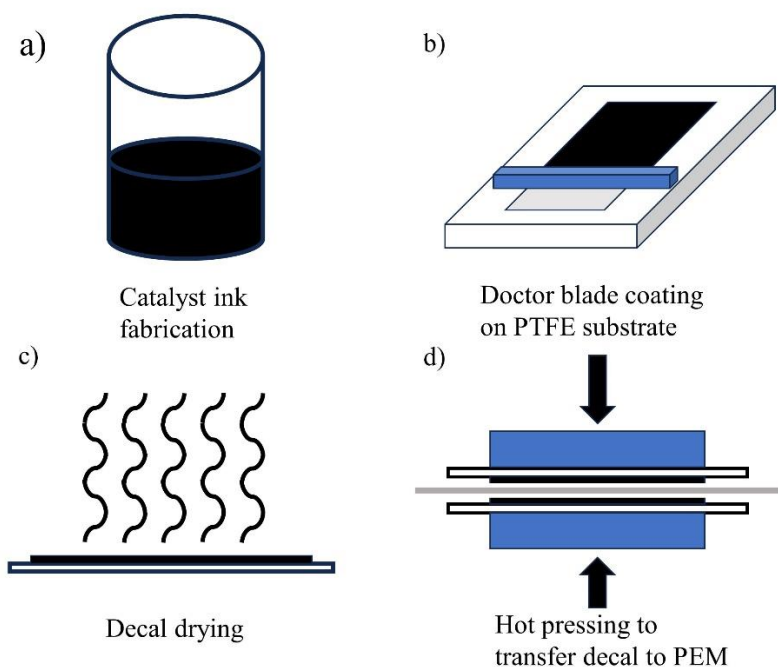


Figure 1.5. Schematic diagram of Decal Transfer Method. The coating process includes a) catalyst ink fabrication; b) doctor blade coating on PTFE substrate; c) decal drying; d) hot pressing to transfer decal to PEM.

Decal transfer method (DTM) is also an important method for the CCM fabrication. DTM (Figure 1.5) usually uses a doctor blade to firstly coat the CL on a temporary substrate (such as

PTFE film). When the catalyst ink dries, intercept the part of decal where the catalyst is evenly distributed, and then transfers the CL from the temporary substrate to the PEM by hot press [24].

Doctor blade can control the thickness of CL more precisely during the coating process, and can choose which region on the decal is being intercepted and transferred. Therefore, compared with other coating methods, DTM has the best controllability and repeatability [24]. Liang et al. [39] optimized the composition of the catalyst ink, drying processes, and transfer pressure to achieve a continuous and uniform catalyst layer. The results indicated that adjusting the solvent composition in the catalyst ink to regulate its viscosity facilitates the uniform spreading of the catalyst ink, thus achieving a consistent thickness of the catalyst layer after drying.

However, the catalyst waste of DTM is a serious problem because the CL on the temporary substrate is usually only partially usable, and this would be a problem in mass production. Therefore, enhancing the transfer efficiency of the catalyst to minimize catalyst loss is a focus of many studies. Ha et al. [40] discussed the impact of different substrates on catalyst transfer efficiency. The results demonstrated that the transfer efficiency using Teflon as a substrate was significantly superior to that using Kapton. Cho et al. [41] developed a liquid nitrogen freezing technique. The results indicated that this method achieved a catalyst transfer efficiency of 99.2%, a substantial improvement over the traditional methods which typically reach 95.4%.

In addition, DTM steps have the need to perform hot press for transfer, and hot press needs to exceed ionomer's glass transition temperature. This does not have much impact on MEA using *Nafion* (T_g is about 130°C) [18], but it is more difficult to apply DTM to MEA using *Pemion* (T_g is about 300°C) [17]. Shahgaldi et al. [42] investigated the use of fluorinated ethylene propylene (FEP) as a decal substrate for low temperature DTM on *Nafion*, but this method still requires

exceeding the glass transition temperature of ionomer and does not address the challenge of high glass transition temperatures of *Pemion* in large-scale DTM production.

1.2.3 Blade Coating Method

The blade coating method (BCM) is a technique that combines the features of ASM and DTM. Similar to DTM, BCM uses a blade to scrape the catalyst ink. The difference is that the DTM uses a doctor blade with a fixed interval height to control the thickness of the CL and scrape the catalyst ink onto the temporary substrate, while BCM uses a fixed thickness of Kapton as a mask to create an interval and use it to control the thickness of CL, and then scrape the catalyst ink directly onto the PEM (Figure 1.7). BCM also has good controllability and repeatability. Liu et al. [43] investigated the effects of the solvent composition of isopropanol/H₂O and the solid content in the catalyst ink on the structure of the catalyst layer. The study indicated that using improving catalyst ink led to the formation of a uniformly distributed anode catalyst layer.

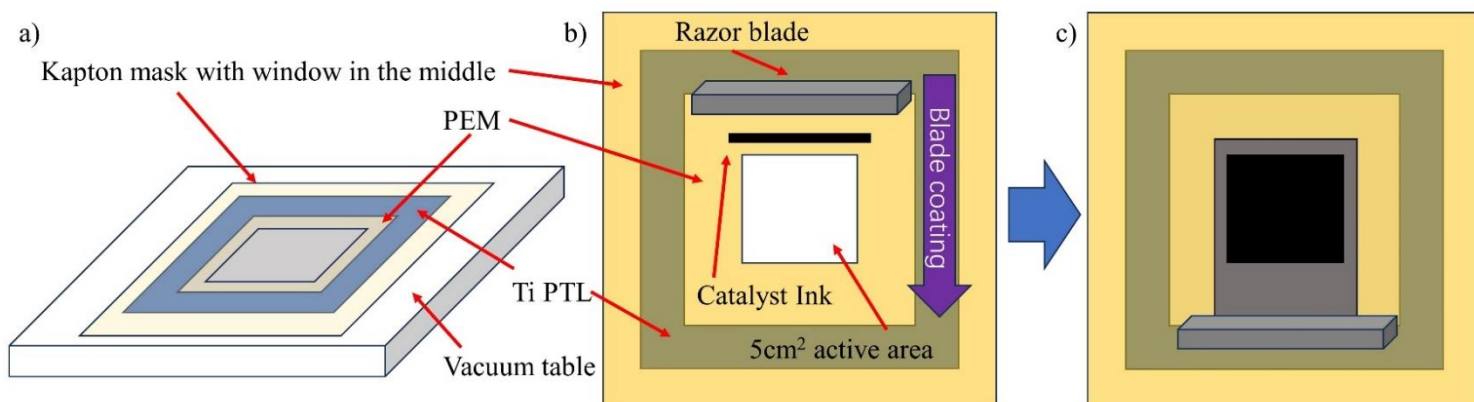


Figure 1.6. Schematic diagram of Blade Coating Method. a) equipment setup; b) blade coating illustration; c) coating effect. The coating area on the PEM was limited by the window on Kapton mask.

Since the interval is fixed, BCM also has good controllability and repeatability. At the same time, because it belongs to direct coating like ACM, BCM has no need for hot press, and is

suitable for *Pemion* CCM fabrication. However, because it is directly scraped onto PEM, BCM cannot intercept the CL part with better uniformity like DTM, so it is difficult to obtain the same CL uniformity as DTM. Park et al. [44] investigated the deformation of the catalyst layer caused by the deformation of the membrane during the coating process. The study revealed that this deformation results from in-plane compression induced by the hydration of the membrane, leading to membrane creep to alleviate these stresses. When catalyst ink is applied to a polymer membrane, both the membrane and the catalyst layer can deform due to rapid volumetric changes. To address this issue, Hsu et al. [45] proposed a process using pre-expanded *Nafion* membranes to reduce stress problems. The study showed that MEAs fabricated from *Nafion* membranes pre-soaked and pre-expanded in ethylene glycol performed approximately 16% better than MEAs without this process. Additionally, Huang et al. [46] investigated the rheological behavior of catalyst inks prepared with different organic solvents, including water, ethylene glycol, glycerol, propylene glycol, and methanol. The research indicated that Pt catalysts and *Nafion* ionomers exhibit better dispersion in ethylene glycol due to its higher dielectric constant and viscosity.

By adjusting the ratio of water and IPA in the solvent, the viscosity of the catalyst ink, the thickness of the Kapton mask, the scraping temperature, the scraping speed, the amount of ink used in a single passing, and many other parameters, BCM can be applied to different types of ionomers after solving the problem of CL uniformity, and it is friendly to large-scale production since the catalyst waste is low. However, current optimization efforts for the Blade Coating Method (BCM) are primarily focused on *Nafion*, with no existing studies on applying BCM to hydrocarbon-based ionomer *Pemion*. Given the lower cost and more environmentally friendly

characteristics of hydrocarbons, researching and optimizing the application of BCM on *Pemion* is highly valuable.

CHAPTER 2: Experimental

The objective of this study is to prepare catalyst coated membrane (CCM) with uniform catalyst layer (CL) by blade coating method (BCM). The target anode catalyst loading is 0.1 mgPt/cm² and the cathode catalyst loading is 0.3 mgPt/cm².

2.1 Equipment and Materials

2.1.1 Materials for CCM Fabrication

For *Nafion*: High surface area carbon-based Pt/C electrocatalyst TEC10E50E was purchased from Tanaka Kikinzoku International Inc., Chicago, Illinois, with a Pt concentration 46.5%. *Nafion* dispersion D521 was purchased from Fuel Cell Store, Bryan, Texas, with a 1100 EW and 5% solid weight. Proton-exchange membrane *Nafion* NR211 was purchased from Ion Power Inc., New Castle, Delaware, with a 1100 EW and 25.4 μm thickness. Gas diffusion layer Freudenberg H23C6 was purchased from Fuel Cell Store, Bryan, Texas, with a manufacturer-reported thickness 250 μm.

For *Pemion*: High surface area carbon-based Pt/C electrocatalyst TEC10E50E was purchased from Tanaka Kikinzoku International Inc., Chicago, Illinois, with a Pt concentration 46.5%. *Pemion* Ionomer PP1-HNN8-00 was purchased from Ionomr Innovations Inc., Vancouver, Canada. *Nafion* decal 1219043 E2 was purchased from 3M, St. Paul, Minnesota, with a 0.4 I/C ratio, catalyst loading 0.1 mgPt/cm², and Vulcan Pt/C catalyst 10V20E. Proton-exchange membrane *Nafion* NR211 was purchased from Ion Power Inc., New Castle, Delaware, with a 1100 EW and 25.4 μm thickness. Gas diffusion layer Freudenberg H23C6 was purchased from Fuel Cell Store, Bryan, Texas, with a manufacturer-reported thickness 250 μm.

2.1.2 Electrochemical Characterization

The fuel cell test fixture suitable for 25 cm² area cells and 850 Fuel Cell Test System were purchased from Scribner Associates, Connecticut, USA. A VSP potentiostat was purchased from Biologic, Knoxville, USA, with a 5 μ V potential resolution and 4 A current maximum.

2.2 Catalyst Ink

In this study, the ionomer to carbon ratio (I/C ratio) of the prepared *Nafion* catalyst ink was 0.9, and the I/C ratio of *Pemion* catalyst ink was 0.3. Inks with different catalyst densities ranging from 4.35 mgPt/mL (5 mgC/mL) to 26.07 mgPt/mL (30 mgC/mL) were prepared, and 17.38 mgPt/mL (20 mgC/mL) was found to be the best. After the introduction of ethylene glycol (EG), we tried to prepare ink with different solvent ratios, including water: isopropyl alcohol: ethylene glycol ratio of 1:1:0/1:1:0.5/1:1:1/1:1:0.3/1:1:0.5 five kinds (Table 3.2). It was found that the catalyst ink with a solvent ratio of 1:1:0.1 had the best coating effect.

2.2.1 Composition

Catalyst ink usually contains supported catalyst particles, ions and solvent.

The supported catalyst particles used in this study were TKK high surface area (TKK HSA) carbon Pt/C catalyst TEC10E50E. Supported catalyst particles are typically made by depositing catalyst on the surface of carbon nanoparticles [25]. HSA carbon can support a higher mass percentage of catalyst compared to Vulkan carbon. Using HSA carbon catalyst can achieve the same catalyst loading with a thinner catalyst layer (CL) [26]. The thickness of CL determines the path length of proton transport and oxygen diffusion, and also affects the removal of reaction product water. Thinner CL can reduce the ohmic overpotential and mass transfer overpotential at high current densities, thereby improving the electrochemical performance [14].

The ionomers used in this study were *Nafion* and *Pemion*. *Nafion* is the most widely used ionomer and is widely used due to its excellent proton conductivity. Based on a similar

polytetrafluoroethylene backbone, *Nafion* is highly chemically and thermally stable, ensuring a longer service life under a variety of conditions [18]. However, because *Nafion* is made from perfluorinated compounds, it would have a significant impact on the environment after retirement. *Pemion* is a hydrocarbon-based ionic polymer developed by Ionomr Innovations. *Pemion* has higher thermal stability and similar proton conductivity compared to *Nafion* [27], and as a hydrocarbon-based ionomer, *Pemion* is more environmentally friendly. In 2023, *Pemion*-based PEMFCs exceeded internationally recognized performance and durability standards set by the U.S. Department of Energy (US DOE) and Hydrogen Europe [27].

The solvent used in this study was a mixture of water, isopropyl alcohol (IPA), and ethylene glycol (EG). Ngo et al. and Yang et al. found that ionomers in hydroalcohol mixtures exist in the form of highly solvated large particles [28] and are adsorbed on the Pt/C surface through van der Waals attraction [29]. After the catalyst ink is applied to the PEM surface, the solvent is evaporated by heat, and the ionomers in the ink act as a binder between Pt/C and PEM [30].

This study found that the viscosity of the catalyst ink has a significant impact on the uniformity of the catalyst layer (CL) prepared by the blade coating method (BCM). Too low a viscosity will cause the catalyst ink to only adhere to certain areas of the proton exchange membrane (PEM) surface after blade passed, while other areas will have no catalyst attached (Figure 2.1a). On the contrast, excessively high viscosity can cause different drying rates after ink application (coffee-ring effect), causing the CL to crack and fall off the PEM after multiple coatings (Figure 2.1b,c).

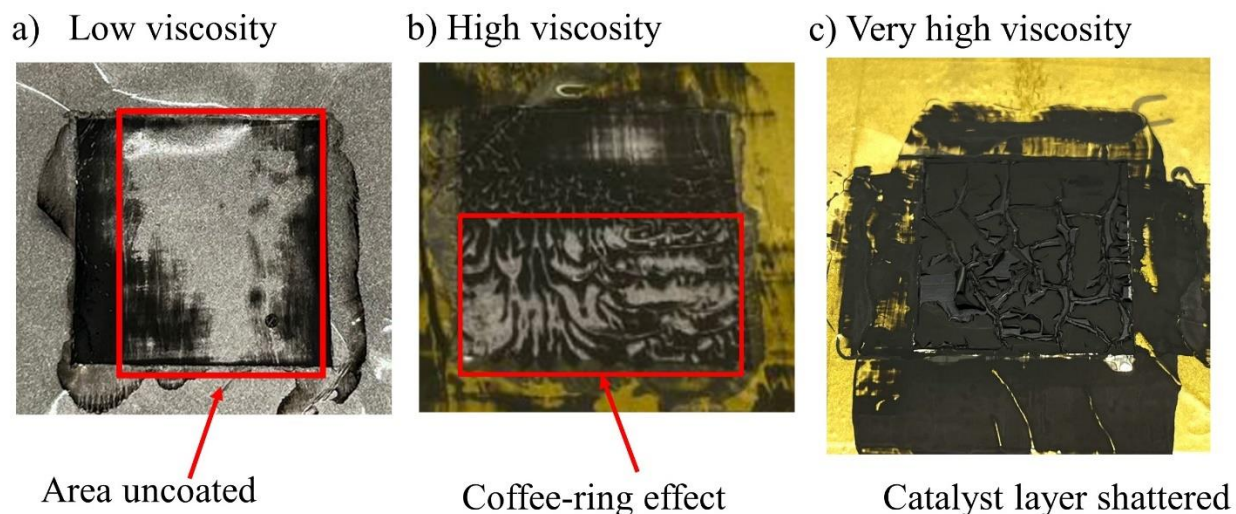


Figure 2.1. Coating effect with different ink viscosity. a) ink with low viscosity resulted in part of the area that was not coated; b) ink with high viscosity resulted in different parts have different drying speeds resulting in coffee-ring effects; c) ink with very high viscosity resulted in a very strong coffee-ring effect leading to the catalyst layer being shattered.

To achieve ideal coating results, the ink volume used for each BCM coating should generally not be less than 50 μ l, as the applied catalyst ink may be depleted before a single scratch is completed, resulting in uncoated areas on the PEM. In addition, in order to achieve a uniform CL distribution, preparation of CCM by BCM usually requires at least four passing (scraping once from each direction of the mask window). At lower target loads, it is necessary to reduce the catalyst density in the catalyst ink to avoid excessive catalyst loading. At a fixed ionomer to carbon ratio (I/C ratio), the amount of ionomer dispersion in the catalyst ink must also be reduced. Since the dispersed content of ionomer is a key parameter in maintaining solution viscosity, reducing ionomer will result in a too low viscosity of the IPA/water solvent. Therefore, it is necessary to introduce ethylene glycol (EG), which has a higher viscosity and does not react with ionomers [31], to adjust the overall viscosity of the catalyst ink.

2.2.2 Fabrication

According to the target catalyst density, an appropriate amount of TKK HSA Pt/C catalyst is added to an 8 mL plastic bottle, followed sequentially by the addition of DI water, IPA, and EG according to the solution ratios. The plastic bottle is then sealed and being ice bath sonicated for 5 minutes. Opening the plastic bottle, ionomer dispersion is added based on the target I/C ratio, and then 8.8 g of zirconia balls are added into the bottle. The bottle is sealed again and placed on a roll miller set at 60 rotations per minute for 24 hours of ball milling. The plastic bottle can be removed from the roll miller and stored for up to two weeks; thereafter, the ink will be retired, and new ink must be prepared. Before using the ink, it requires ice bath sonicating for 20 minutes.

2.3 Procedure of Blade Coating

A vacuum table is heated to 60°C using a heating block. Another heating block is set to 110°C on the side. A razor blade, cleaned with IPA, is preheated on the vacuum table.

A 5 cm x 5 cm piece of *Nafion* NR211 PEM is cut, the protective film is removed, and its weight is recorded as m_1 . A 6 cm x 6 cm titanium porous transport layer (PTL) is placed on the vacuum table. A 5 cm x 5 cm piece of *Nafion* NR211 PEM is cut, the protective film is removed, and its weight is recorded as m_1 . The PEM is placed on the PTL. A 6.5 cm x 6.5 cm piece of Kapton, with a thickness of 25 μm , is cut, and a window measuring 2.23 cm x 2.23 cm is carved in the center. The PEM is then covered with the Kapton mask, restricting the effective coating area to 5 cm^2 . The vacuum valve is opened, and 50 μL of catalyst ink is transferred to a position approximately 2-3mm from the window on the Kapton mask using a micropipette, and a line slightly longer than the window is drawn with the ink. The ink is then scraped across the window of the Kapton mask with the preheated razor blade, the duration controlled to approximately 2 seconds. Approximately 1 minute later, the vacuum valve is closed, and the PTL-PEM-mask

assembly is placed on the other heating block preheated to 110°C for 10 minutes to facilitate evaporation of most of the solvent. Once drying is complete, the PEM is removed, weighed, and the weight m_2 is recorded to estimate the catalyst loading by Δm . This procedure is repeated until the target catalyst loading is reached. Each placement of the PEM involves a 90° rotation to alter the direction of the coating, aiding in achieving a more uniform CL structure.

When the desired catalyst loading reached, the CCM is placed in a 90°C vacuum oven overnight to maximize the removal of residual EG. After vacuum drying, the actual catalyst loading is accurately measured using an X-Ray Fluorescence machine.

2.4 Electrochemical Characterization

Cyclic voltammetry (CV) is utilized to understand the basic characteristics of the membrane electrode assembly (MEA) and to estimate the electrochemical active surface area (ECSA). Measurements are conducted at a scan rate of 20 mV/s, within a voltage range of 0.05 V to 1.00 V, with an anode flow rate of 0.2 standard liters per minute (slpm) hydrogen, and a cathode flow rate of 0.2 slpm nitrogen. Linear sweep voltammetry (LSV) is employed to measure hydrogen crossover, with a scan rate of 1 mV/s, scanning from 0.05 V to 0.80 V, and an anode flow rate of 0.3 slpm hydrogen and a cathode flow rate of 0.3 slpm nitrogen. Electrochemical impedance spectroscopy (EIS) is used to understand information such as high-frequency resistance (HFR), scanning from 0.1 Hz to 20 kHz at 6 points per decade, with an anode flow rate of 1 slpm hydrogen and a cathode flow rate of 1 slpm nitrogen. CO stripping is used to precisely calculate ECSA and SO₃ group coverage, with an anode flow of 1 slpm of 5% hydrogen/95% nitrogen. CO Stripping involves three steps: CO displacement, CO stripping, and a CV. During the CO displacement step, the voltage is maintained at 0.35 V, and the cathode flow is 1 slpm nitrogen. After two minutes, the cathode flow is replaced with 1 slpm of 2% CO/98% nitrogen for five

minutes. In the CO stripping step, the cathode flow is switched back to 1 slpm nitrogen, the voltage is held at 0.2 V for twenty minutes, followed by a CV scan at a rate of 40 mV/s, within a range of 0.05 V to 1.00 V. All electrochemical characterizations are conducted at 80°C, 100% relative humidity (RH), and atmospheric pressure using a VSP potentiostat from Biologic.

Cell conditioning is carried out to promote membrane hydration, catalyst activation, and gradual load cycling to adapt the materials to operational stresses. Conditioning aids in achieving consistent and reliable performance from the onset of fuel cell usage. This procedure cycles the voltage between 0.8 V, 0.5 V, and 0.2 V, maintaining each stage for 30 seconds over 100 cycles, with an anode flow of 0.6 slpm hydrogen and a cathode flow of 1 slpm air, conducted at 80°C, 100% RH, and a back pressure of 150 kPa. Voltage recovery is used to generating a substantial amount of water to clear blocked flow channels, remove contaminants, and rehydrate the membrane. This procedure maintains the voltage at 0.1 V for 5400 seconds, with an anode flow of 0.1 slpm hydrogen and a cathode flow of 0.1 slpm air, at 40°C, 150% RH, and a back pressure of 150 kPa. The polarization curve is used to understand the overall performance of the cell and the activation/ohmic/transport overpotentials. This procedure starts with the highest current achievable by the MEA, maintaining the cell under constant current for three minutes during which six voltage readings are taken, then reducing the current by 0.5 A and continuing with constant current/voltage measurements until reaching 0 A, with an anode flow of 0.5 slpm hydrogen and a cathode flow of 1.2 slpm air, at 80°C, 100% RH, and a back pressure of 150 kPa. The average voltage of each stage is taken to obtain the polarization curve. Mass activity measurements are used to understand the conditions of the MEA in the activation area. This procedure maintains the voltage at every 0.1 V interval from 0.75 V to 0.92 V for three minutes and records the current, with an anode flow of 1 slpm hydrogen and a cathode flow of 2.5 slpm

oxygen, at 80°C, 100% RH, and a back pressure of 150 kPa. Limiting current test is employed to calculate the oxygen mass transport resistance [32,33]. This procedure scans from 0 V to OCV at rates of 5/10 mV/s and records the current, at 80°C, 60%/75%/80%/100% RH, and back pressures of 150/250/350 kPa, with an anode flow of 1 slpm hydrogen and a cathode flow of 4 slpm 1%-5% oxygen/99%-95% nitrogen. A Scribner test stand is used for the aforementioned electrochemical analyses.

Upon the completion of a new MEA, an initial set of CV and LSV tests is conducted to check for any serious issues with the MEA. If the data are normal, one cell conditioning procedure and several voltage recovery procedures are performed. Subsequently, Begin of life (BOL) testing is conducted, which includes successive tests of CV, LSV, EIS, polarization curve, mass activity, CO stripping, and limiting current test. Since this study does not involve MEA degradation, accelerated stress tests related to degradation will not be conducted.

2.5 Electrochemical Data Analysis

The electrochemically active surface area (ECSA) of a catalyst can typically be determined by two methods [34]: based on the hydrogen underpotential deposition (H_{UPD}) charge from cyclic voltammetry (CV) graphs and CO stripping. Both methods calculate ECSA using the same formula (Formula 2.1), although some constants differ.

$$ECSA = \frac{\int i dE}{\nu * L * A * C} \quad 2.1$$

When calculating ECSA via H_{UPD} , the current in the H_{UPD} region on the MEA's CV is integrated, subtracting the baseline corresponding to the H_{UPD} region, to obtain the integral $\int i dE$ in the formula (Figure 2.2a). The H_{UPD} region spans from the onset of hydrogen evolution to the double layer capacity. In calculating ECSA via CO stripping, the integral of the difference in current between the first and subsequent CV scans is taken to obtain $\int i dE$ in the formula (Figure

2.2b). In the formula, A is active area, L represents the catalyst loading, ν is the scan rate, and C is the Pt unit charge, taken as $210 \mu\text{C}/\text{cm}^2$ for H_{UPD} calculations and $420 \mu\text{C}/\text{cm}^2$ for CO stripping calculations.

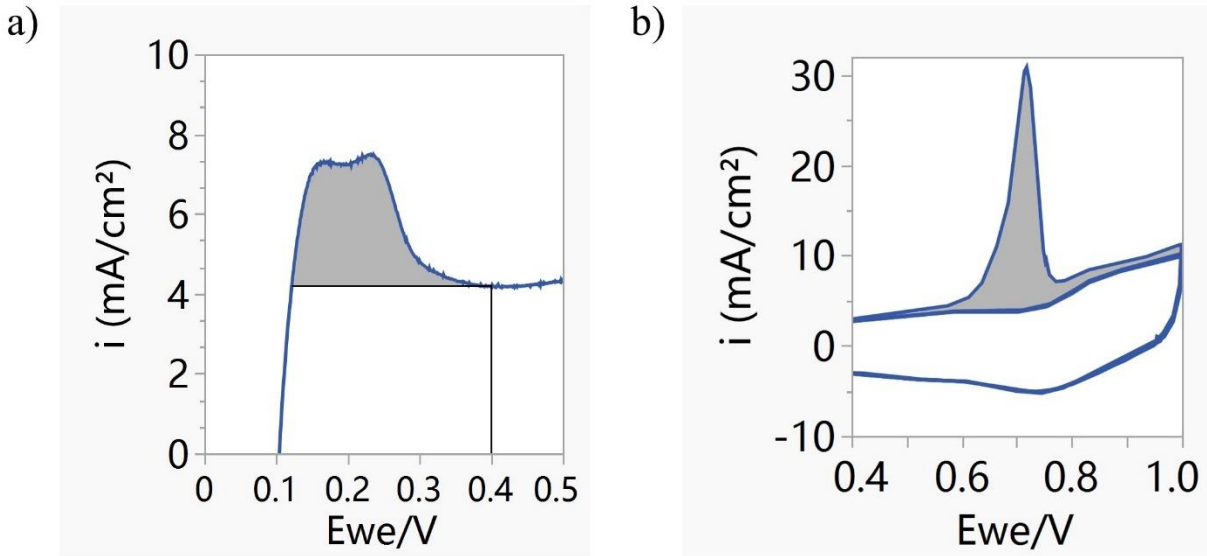


Figure 2.2. Integral area (gray) for a) H_{UPD} and b) CO stripping when calculating ECSA.

The hydrogen crossover current density (HCCD) of a MEA is measured using LSV. This data is commonly used to ascertain whether the MEA has been assembled correctly, whether there is damage to the CCM, and whether there are any shorts in the system. The current at a voltage of 0.3 V during the LSV is taken to determine the HCCD of the MEA at that point. For MEAs using Nafion NR211 as the PEM, it is generally considered that an HCCD below 2 mA/cm² indicates the MEA is performing as expected. Additionally, observing the slope of the LSV from 0.3 V to 0.8 V can provide insights; if the slope is relatively flat (for example, if the HCCD remains below 2 mA/cm² at 0.8 V), it suggests that the CCM is intact and there are no shorts within the system. Furthermore, HCCD is also used as a correction parameter in the polarization curve calculations of the MEA to obtain more accurate Tafel slopes and exchange current densities.

High-frequency resistance (HFR) is another correction parameter for the polarization curve, typically obtained through electrochemical impedance spectroscopy (EIS). The HFR under specific conditions is determined by the x-intercept of the measured EIS data in a Nyquist plot. Additionally, when measuring the polarization curve using a Scribner Test Stand, the corresponding HFR is also recorded.

When calculating the oxygen transport resistance (OTR), firstly measure the limiting current, then use the following formula (Formula 2.2) to obtain R_t for each back pressure (BP) and oxygen concentration.

$$R_t = \frac{C_0 * 4 * F}{I_L}, \text{ where } C_0 = \frac{P - P_W}{RT} * X_0 \quad 2.2$$

Take an average R_t for each BP level, and plot BP vs. R_t , then fit a line for this plot. OTR can be obtained by taking the y-intersect of the fitting line.

The number 4 refers to the number of electrons involved in the oxygen reduction reaction (ORR), and F denotes Faraday's constant. I_L represents the limiting current, C_0 represents the actual concentration of oxygen at the cathode, P refers to the total pressure of the gas mixture, P_W denotes the partial pressure of water vapor, and X_0 indicates the mole fraction of oxygen in the gas mixture. Additionally, the limiting current is also used in the calculation of concentration overpotentials.

Performance measurement of proton exchange membrane fuel cells (PEMFCs) is typically conducted via polarization curves. These curves can generally be divided into three regions: the activation region, ohmic region, and mass transport region. Activation polarization usually occurs at the electrode-electrolyte interface (triple phase boundary, TPB) and is significantly influenced by the exchange current density. In H₂-O₂ fuel cells, the kinetics of the hydrogen oxidation reaction (HOR) are typically fast, thus the rate-limiting step is often the kinetics of the

oxygen reduction reaction (ORR). Therefore, if an MEA exhibits significant activation overpotential, it might indicate a scarcity of possible reaction sites at the cathode. This situation often arises with uneven distribution in the catalyst layer (CL). Since the objective of this study is to produce a uniform CL, the activation overpotential of an MEA can be considered an indicator of the quality of the coating effect. Ohmic polarization loss is primarily affected by the total cell resistance and can be reduced by using a thinner PEM or a higher electrode catalyst loading. Since the PEM and target catalyst loading in this study are fixed, significant changes in ohmic polarization loss are not anticipated. Mass transport polarization primarily results from the mass transfer of reactants and products at the TPB. Thinner and more porous CLs can enhance the supply of reactants, thus reducing mass transport polarization loss. This study found that CCMs prepared via BCM often exhibit higher mass transport region losses compared to those prepared by ASM. However, this was improved after multiple voltage recovery cycles, suggesting that residual EG on the new CCM may be blocking some channels in the CL.

CHAPTER 3: Results and Discussion

3.1 Nafion MEA

This study on the preparation of *Nafion*-based catalyst coated membranes (CCMs) primarily consists of three stages: achieving the target catalyst loading, enhancing the uniformity of the catalyst layer (CL), and producing a CCM with electrochemical performance comparable to those prepared by the air-spraying method (ASM). The research explores the impact of catalyst density in the ink, solvent ratios, and coating methods on the coating effect and electrochemical performance. As a standard for comparing the performance across different MEAs, the current density at 0.7 V from HFR-corrected polarization curves is used as a reference. For ASM-prepared CCM, the current density at 0.7 V is 0.4 A/cm².

3.1.1 Ink Configuration and Coating Effects

The catalyst density in the catalyst ink plays a crucial role. This study uses a fixed ionomer to carbon (I/C) ratio of 0.9 for *Nafion*, thus adjusting the catalyst density directly affects the ionomer content in the ink. The ionomer in the ink acts as an adhesive between the catalyst particles and the PEM, with its content directly influencing the coating effect.

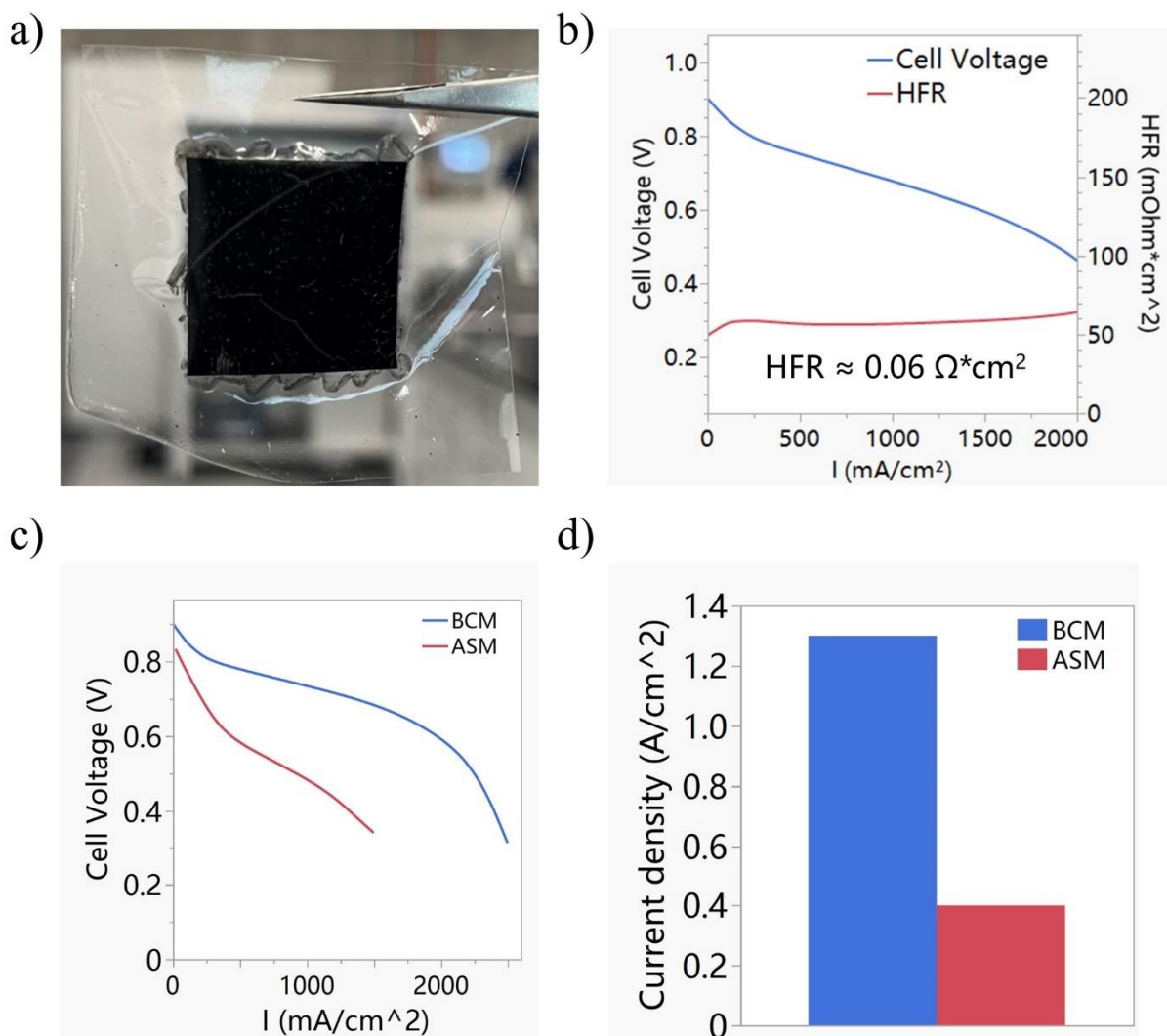


Figure 3.1. a) CCM made by BCM with 0.95 mgPt/cm^2 ; b) polarization curve and HFR data; c) comparison of HFR-corrected polarization curve of BCM-prepared CCM and an ASM-prepared benchmark CCM with 0.378 mgPt/cm^2 catalyst loading on cathode; d) comparison of HFR-corrected current density at 0.7V. Under this high catalyst loading, good CCM can be easily fabricated by BCM.

The study initially focuses on preparing CCMs with a higher catalyst loading. Using an ink with a catalyst density of 26.07 mgPt/mL , and after 8 coatings of $75 \mu\text{L}$ each on an 80°C vacuum table, a CCM with a catalyst loading of 0.95 mgPt/cm^2 was produced, featuring a uniform CL distribution and viable electrochemical performance (Figure 3.1). Adjustments to catalyst density

and the number of passes were made (Table 3.1), and using an ink with a catalyst density of 8.69 mgPt/mL, a CCM with a catalyst loading of 0.28 mgPt/cm² was prepared after 4 coatings of 50 μL each. Electrochemical characterization revealed a normal ECSA of 43.95 m²/g but significant activation polarization loss (Figure 3.2), indicating the CCM lacked viable fuel cell performance.

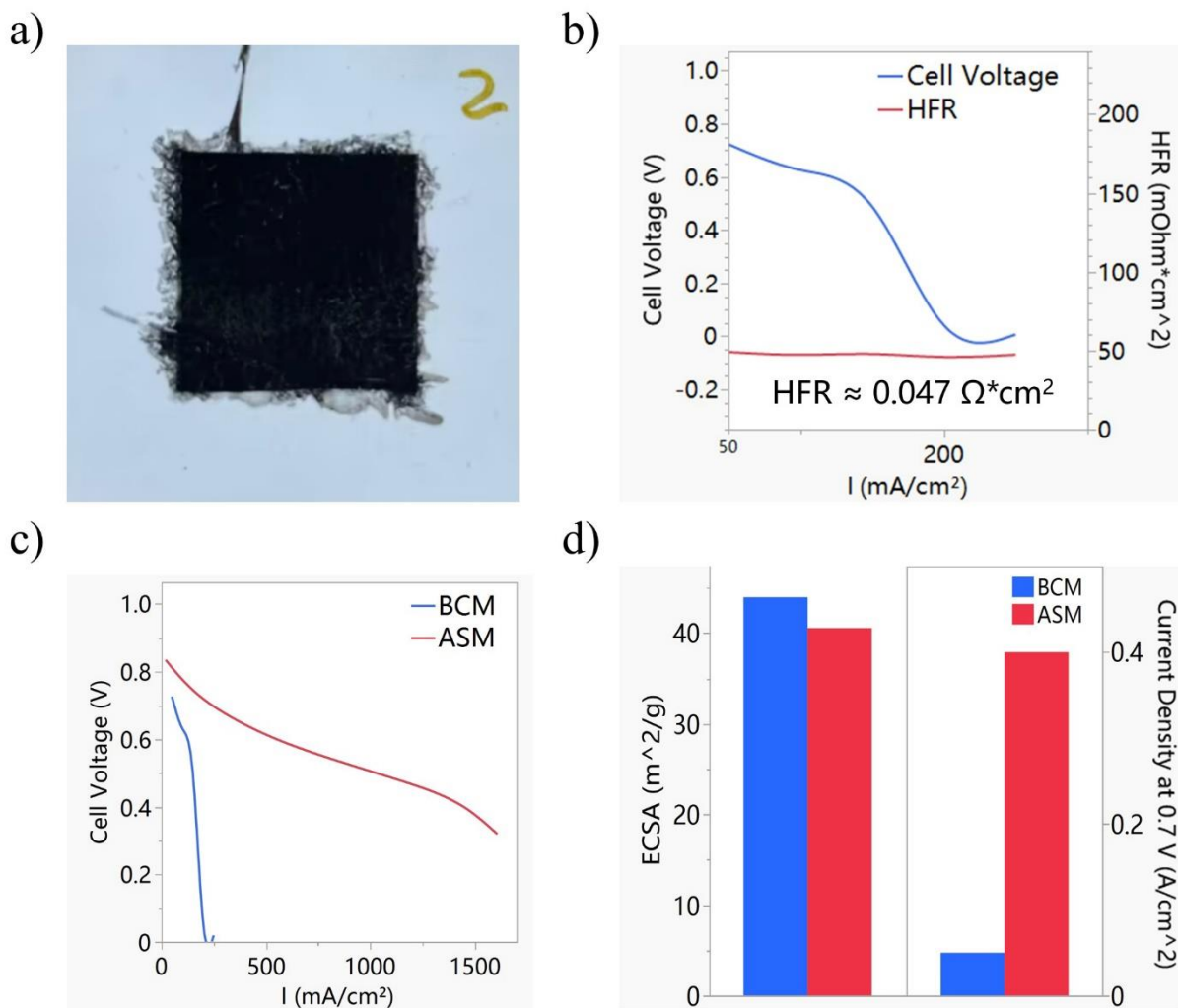


Figure 3.2. a) CCM made by BCM with 0.28 mgPt/cm²; b) polarization curve and HFR data; c) comparison of HFR-corrected polarization curve of BCM-prepared CCM and an ASM-prepared benchmark CCM with 0.378 mgPt/cm² catalyst loading on cathode; d) comparison of ECSA and HFR-corrected current density. For this CCM, the ECSA was fine, but the activation loss was significantly higher than ASM-prepared CCM.

Attempts	Coat Temp (°C)	Ink density (mgPt/mL)	Number of Passing	Ink Volume per pass	Cathode Catalyst Loading (mg/cm ²)	Notes
1	80	26.07	8	75 uL	0.98	First CCM with uniform CL, but shorted
2	80	26.07	8	75 uL	0.95	First CCM with electrochemical performance
3	80	26.07	4	50 uL	0.52	Tried to reduce catalyst loading by reduce passings
4	80	8.69	8	50 uL	0.55	Tried to reduce catalyst loading by reduce ink density
5	60	8.69	8	50 uL	0.27	Tried to reduce catalyst loading by lower coating temp
6	60	17.38	4	50 uL	0.34	Loading stable, but high activation polarization loss

Table 3.1. Attempts to reach target cathode catalyst loading 0.3 mgPt/mL.

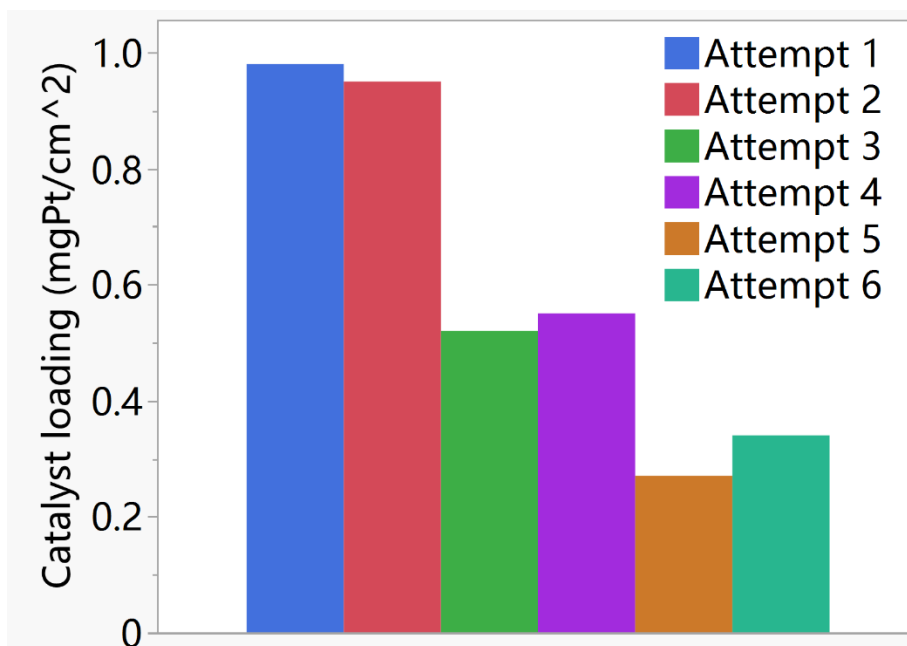


Figure 3.3. Catalyst loading for each attempt in Table 3.1. The target loading is 0.3 mgPt/cm², and this can be reached ($\pm 10\%$) by BCM runs on 60°C vacuum plate, using ink with 17.38 mgPt/mL to coat for 4 passes with 50uL each time.

Furthermore, visibly uneven distribution of the CL was observed, particularly as a single pass often only coated part of the PEM, leaving other areas uncoated (Table 3.2). To address this issue, attempts were made to further reduce catalyst density and increase the number of coatings, aiming to enhance the uniformity of the CL through more passes. Using an ink with a catalyst density of 4.35 mgPt/mL, and after 8 coatings of 50 μ L each, a CCM with a catalyst loading of 0.24 mgPt/cm² was prepared. The overly diluted ink and repeated application of excessive ink led to prolonged contact of the IPA solvent with the PEM, dissolving some of the ionomer and damaging the PEM structure, resulting in significant elongation (Figure 3.4). The prepared CCM exhibited high hydrogen crossover (\sim 3.5 mA/cm² at 0.3 V) and a pronounced slope in the LSV curve, suggesting that elongation of the PEM had caused a short circuit in the MEA.

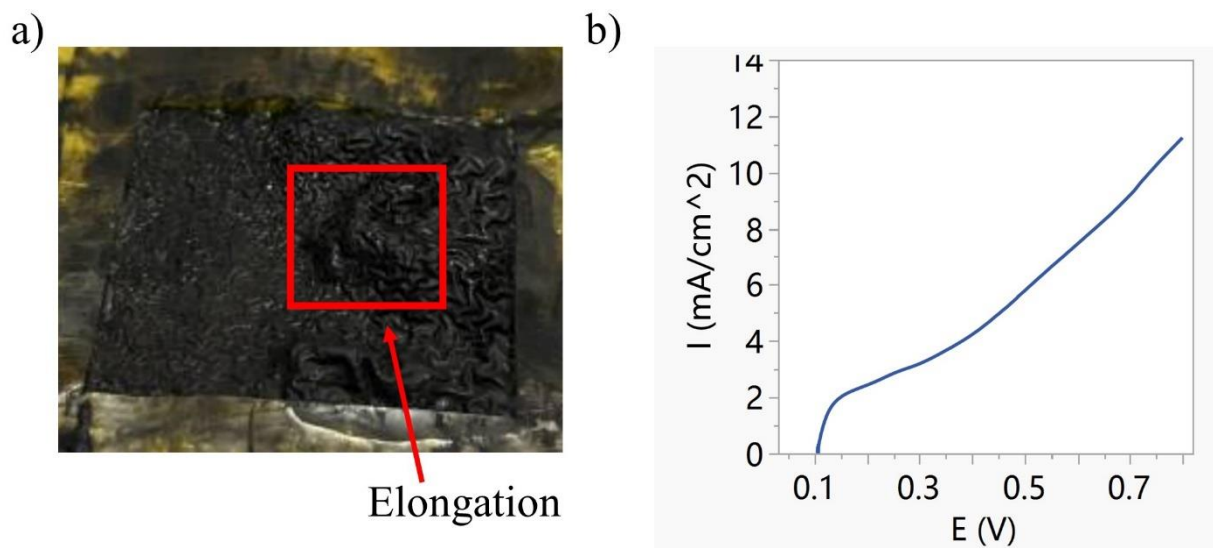


Figure 3.4. a) CCM made by BCM with 0.24 mgPt/cm²; b) LSV data for this CCM. Significant elongation was found when doing BCM. The LSV curve shows a noticeable slope, which proved the structure of CCM has being damaged by applying ink repeatedly and generously to the PEM.

Therefore, attempts to reduce catalyst density in the ink and increase the number of coatings proved to be an unfeasible optimization strategy. To achieve more uniform CL, it was found that

improving each individual coating to ensure uniform coating effects is the correct approach. Tests showed that lowering the coating temperature could effectively reduce the catalyst loading of the CCM (Figure 3.5). However, excessively low temperatures also caused slow evaporation of the IPA in the ink, resulting in greater damage to the PEM. After testing, the new coating temperature was set at 60°C.

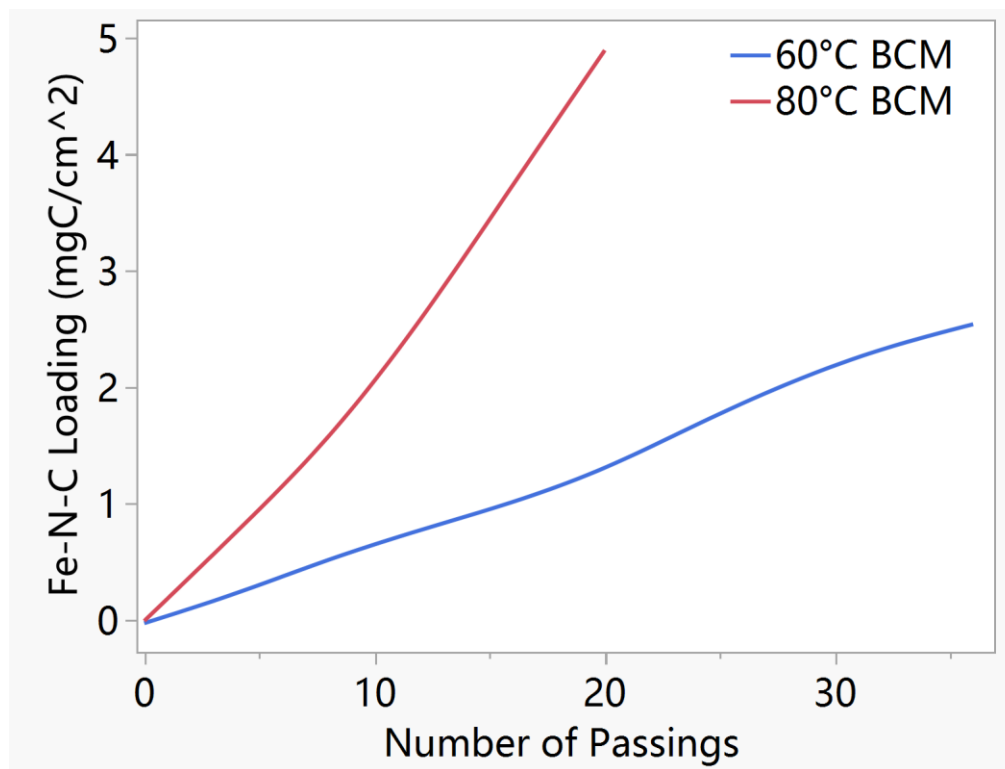
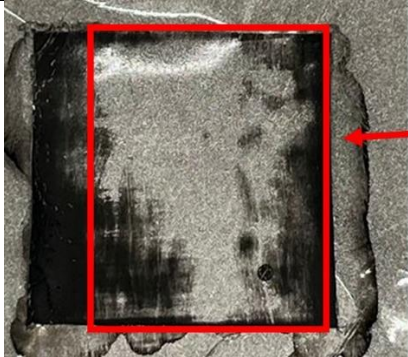
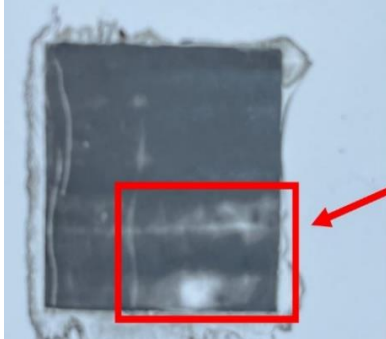
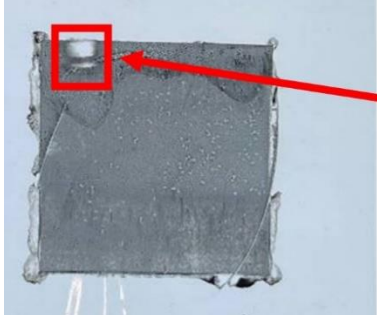


Figure 3.5. Catalyst loading on CCMs using the same ink, but with different coating temperatures. The slope of 80°C BCM is close to two times that of the 60°C BCM. This shows that a lower coating temperature can reduce the catalyst loading by using the same ink.

Additionally, tests altering the I/C ratio in the catalyst ink showed that a higher ionomer content in the ink made individual coatings more uniform, suggesting that better coating effects from high-density ink might be due to higher ink viscosity. As this study aimed to prepare CCM with an I/C ratio of 0.9, altering the ionomer content was not an option. Therefore, attempts were made to introduce ethylene glycol to adjust the ink's viscosity. Catalyst inks with a density of

17.38 mgPt/mL and solvent ratios of DI water:IPA:EG at 1:1:0.1 and 1:1:0.5 were prepared and used in BCM. The viscosity of solvent can be calculated by Formula 3.1, where μ represents viscosity, x represents the mole fraction.

$$\mu_{mix} = \left((x_{water}\mu_{water})^{1/3} + (x_{IPA}\mu_{IPA})^{1/3} + (x_{EG}\mu_{EG})^{1/3} \right)^3 \quad 3.1$$

Solvent Ratio	Viscosity (cP) at 25°C	CCM Loading (mgPt/cm ²)	CCM image for first passing
1:1:0	1.216	0.27	 <p>Large area uncoated</p>
1:1:0.05	1.269	0.29	 <p>Smaller area uncoated</p>
1:1:0.1	1.323	0.26	 <p>Acceptable uncoated area</p>



1:1:0.3	1.53	0.31		<p>Coffee-ring effect</p>
1:1:0.5	1.734	0.33		<p>Catalyst layer shattered</p>

Table 3.2. Attempts to achieve different solvent ratios. The images on the fourth column show a trend of the single pass BCM coating dependence upon viscosity. When viscosity goes lower, a larger part of PEM will not be coated after blade runs by. When viscosity goes higher, a stronger coffee-ring effect will happen.

Adding EG to the solvent allowed each pass to coat all areas of the PEM, but the 1:1:0.5 ink exhibited a significant coffee-ring effect during BCM, leading to catalyst layer cracking and detachment from the PEM after multiple passes, likely due to too high viscosity causing uneven liquid evaporation. The 1:1:0.1 version performed well, with a very uniform CL. Subsequent tests (Table 3.2) with solvent ratios of 1:1:0.05 and 1:1:0.3 found that the 1:1:0.05 ink still left some PEM areas uncoated, while the 1:1:0.3 ink showed a relatively less pronounced coffee-ring effect. This suggested that a DI water:IPA:EG ratio of 1:1:0.1 is an optimal solvent mixture.

After tuning all parameters, the final catalyst ink formulation used had a density of 17.38 mgPt/mL and a solvent ratio of DI water:IPA:EG at 1:1:0.1. During BCM at 60°C on a vacuum

table, using a 25 μm thick Kapton as a mask, and 50 μL of ink for 4 passings, a cathode catalyst loading of $0.26 \text{ mgPt}/\text{cm}^2$ was achieved, and the CCM was assembled as MEA for electrochemical analysis.

3.1.2 Electrochemical Characterization

After assembling the CCM prepared via BCM into a MEA, it is tested using CV and LSV on a Scribner test stand. In pre-conditioning tests, the ECSA calculated via HUPD was $39.56 \text{ m}^2/\text{g}$. The hydrogen crossover current density at 0.3 V was $1 \text{ mA}/\text{cm}^2$, indicating the MEA was in good condition. This was followed by cell conditioning and voltage recovery procedures. After completion, BOL tests were conducted (Figure 3.6). In the BOL tests, the ECSA calculated via HUPD was $45.65 \text{ m}^2/\text{g}$, and via CO stripping was $52.63 \text{ m}^2/\text{g}$, consistent with expectations for a TKK HSA Carbon Pt/C catalyst. The hydrogen crossover current density at 0.3 V remained at $1 \text{ mA}/\text{cm}^2$, and the LSV showed no significant slope. EIS measured at 35°C , 100% RH, with an anode/cathode gas flow of 1 slpm hydrogen/1 slpm nitrogen at atmospheric pressure, gave a HFR of $0.3 \text{ Ohm}\cdot\text{cm}^2$. Subsequently, polarization curves and limiting currents were obtained and compared with data from CCMs prepared by ASM.

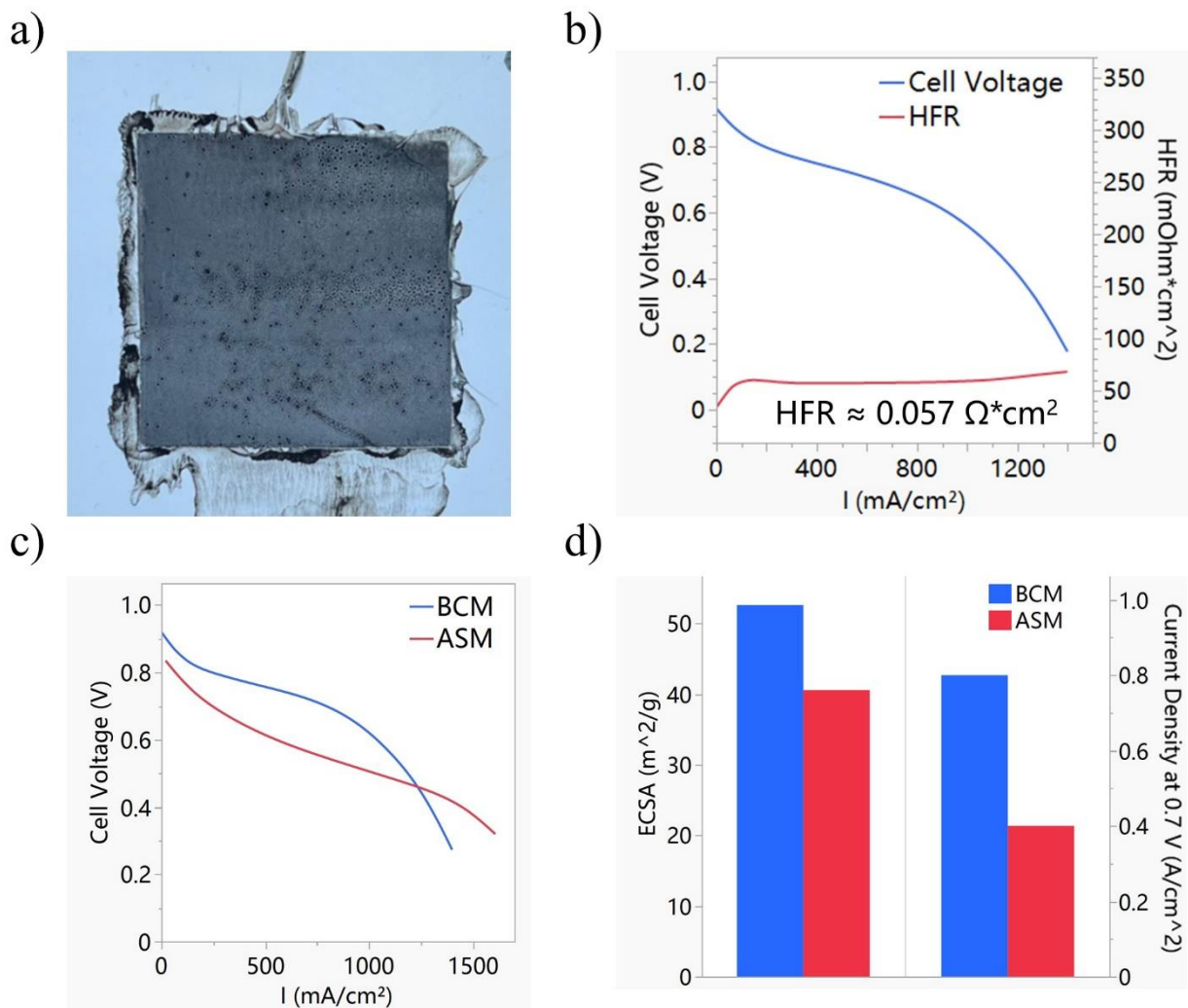


Figure 3.6. a) CCM made by BCM with $0.26 \text{ mgPt}/\text{cm}^2$; b) polarization curve and HFR data; c) comparison of HFR-corrected polarization curve of BCM-prepared CCM and an ASM-prepared benchmark CCM with $0.378 \text{ mgPt}/\text{cm}^2$ catalyst loading on cathode; d) comparison of ECSA and HFR-corrected current density. CCM coated on 60°C vacuum table, with catalyst ink using 1:1:0.1 water:IPA:EG. This CCM shows good ECSA and cell performance, and is the Nafion benchmark for BCM.

The CCMs prepared via ASM, using the same catalyst, GDL, and PEM, had the same I/C ratio and a slightly higher catalyst loading ($0.378 \text{ mgPt}/\text{cm}^2$). Compared to the CCM prepared by ASM (Figure 3.6b), CCM prepared by BCM exhibited relatively lower activation polarization

loss, indicating a more uniform distribution of the CL. The ohmic polarization losses were similar for both, which was expected since the same PEM and catalyst were used. The mass transport polarization loss was noticeably higher for the CCMs prepared by BCM, potentially due to lower porosity and permeability of the electrodes.

After an additional three voltage recovery cycles for the BCM-prepared CCM, the mass transport polarization loss was reduced but still differed from that of the ASM-prepared CCM (Figure 3.7). In the limiting current test, the OTR of the BCM-prepared CCM at 75% RH was 0.669 s/cm (Table 2.1), close to the 0.681 s/cm of ASM-prepared CCM.

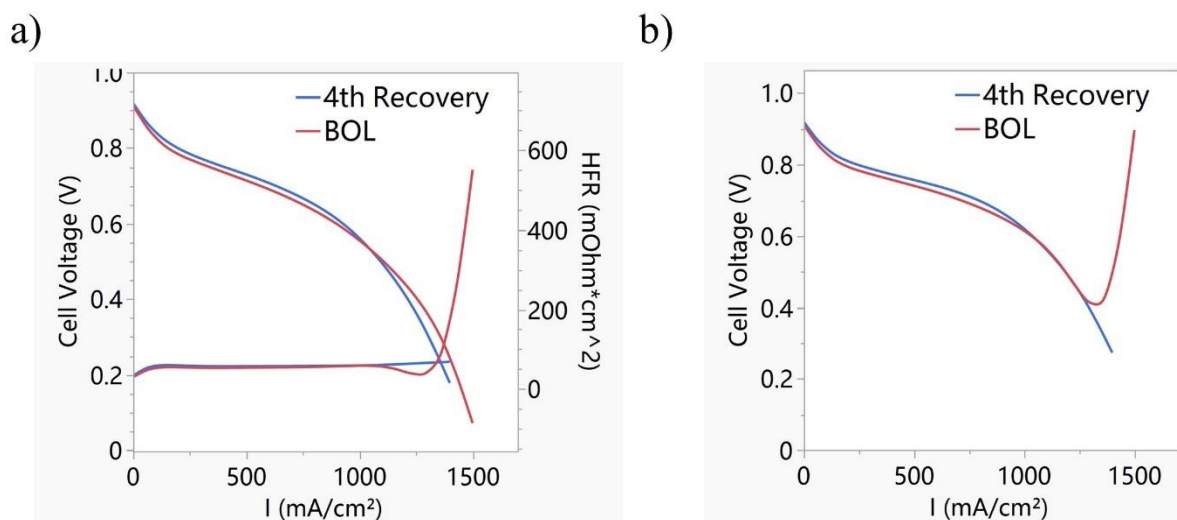


Figure 3.7. Comparison of a) polarization curve and HFR data; b) HFR corrected polarization curve between BOL and after four times voltage recovery. Note that at high current density for BOL, there is a significant rise in HFR. This can be caused by the existence of EG residual. After recovery cycles, the EG residual was removed, so that the high current density rise in HFR disappeared.

3.2 Pemion MEA

After successfully achieving the desired results with *Nafion* MEAs prepared via the BCM, this study also employed BCM to fabricate *Pemion* MEAs. For CCMs using *Pemion* as the

ionomer, I/C ratio of 0.3 was utilized. This lower ratio was necessary because hydrocarbon ionomers are prone to excessive swelling upon hydration, which can stress the catalyst layer and lead to mechanical degradation over time. The target cathode catalyst loading was the same as for the *Nafion* CCM, at 0.3 mgPt/cm². For ASM-prepared *Pemion* CCM, the current density at 0.7 V is 0.8 A/cm².

During the preparation of the *Pemion* CCM, a solvent ratio of DI water:IPA:EG 1:1:0.3 was initially tested for the catalyst ink. Similar to the *Nafion* CCM, a coffee-ring effect occurred (Figure 3.8).

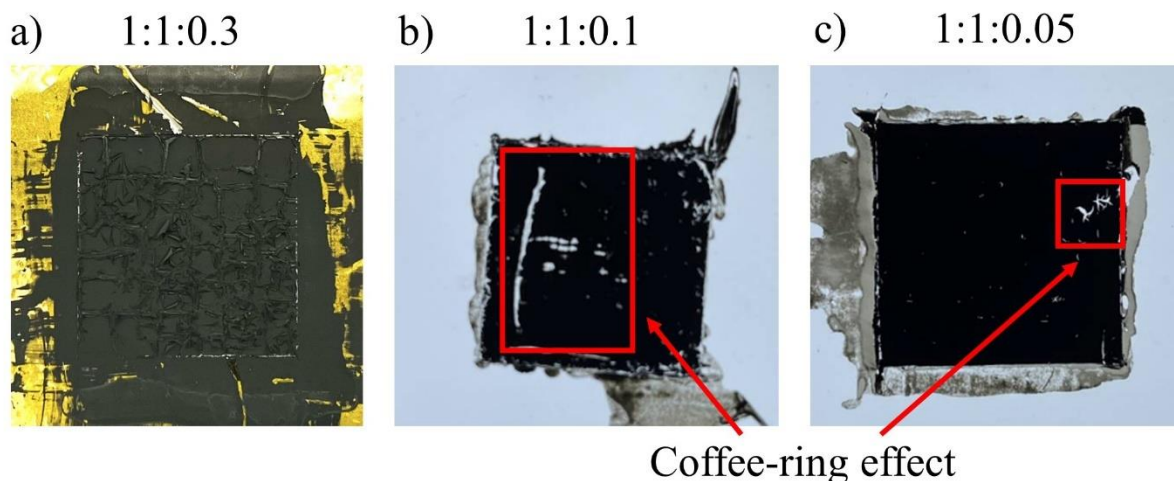


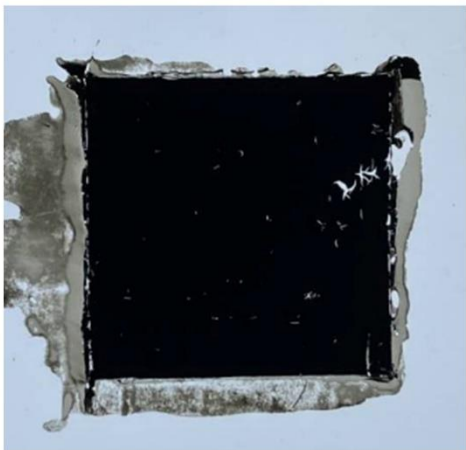
Figure 3.8. *Pemion* CCM coated by catalyst ink with a solvent ratio of water:IPA:EG a) 1:1:0.3; b) 1:1:0.1; c) 1:1:0.05. Note that coffee-ring effects were found on all of these three CCM. For 1:1:0.3, the CL was shattered by coffee-ring effect during drying. For 1:1:0.05, the effect is acceptable, but for future CCM, an even lower EG ratio should be used.

The EG content was then reduced to 1:1:0.1, which improved the situation but still resulted in minor damage to the CL. Eventually, adjusting the solvent ratio to 1:1:0.05 achieved better results, possibly due to the *Pemion* dispersion contributing more viscosity than *Nafion*. The final catalyst ink used had a density of 17.38 mgPt/mL and a solvent ratio of DI water:IPA:EG

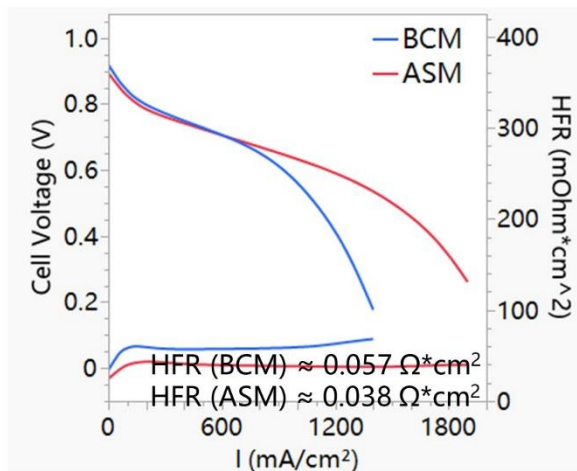
1:1:0.05. During BCM, using a 25 μm thick Kapton mask on a 60°C vacuum table, 50 μL of ink was used for four passings to prepare a CCM with a cathode catalyst loading of 0.21 mgPt/cm^2 , which was then assembled into an MEA and subjected to electrochemical analysis.

After assembling the BCM-prepared CCM into an MEA, it was tested using CV and LSV on a Scribner test stand. In pre-conditioning tests, the ECSA calculated via HUPD was 56.89 m^2/g . The hydrogen crossover current density at 0.3 V was 1 mA/cm^2 , indicating the MEA was in good condition. This was followed by cell conditioning and three voltage recovery procedures. Afterward, BOL tests were conducted (Figure 3.9).

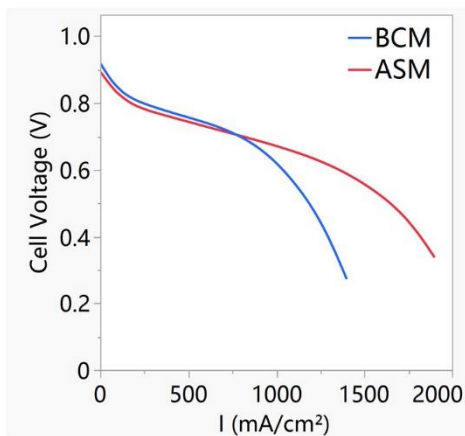
a)



b)



c)



d)

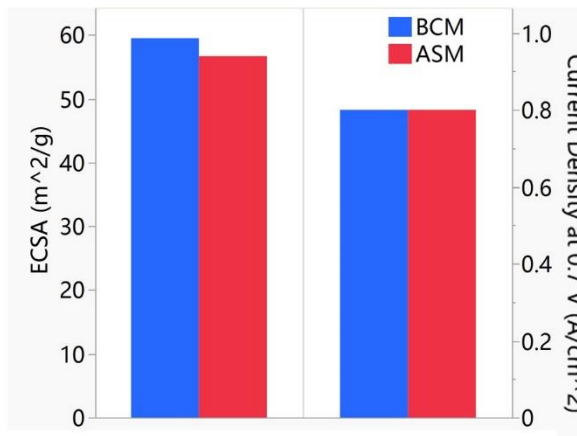


Figure 3.9. a) CCM made by BCM with 0.21 mgPt/cm²; b) polarization curve and HFR data; c) comparison of HFR-corrected polarization curve of BCM-prepared CCM and an ASM-prepared benchmark CCM with 0.372 mgPt/cm² catalyst loading on cathode; d) comparison of ECSA and HFR-corrected current density. CCM coated on 60°C vacuum table, with catalyst ink using 1:1:0.05 water:IPA:EG. This CCM shows good ECSA and cell performance, but it is noticeable that the mass transport loss is higher than the ASM-prepared CCM.

In BOL tests, the ECSA calculated via CO Stripping was 59.5 m²/g, consistent with expectations for a TKK HSA Carbon Pt/C catalyst. The hydrogen crossover current density at 0.3 V was 1.7 mA/cm², but the LSV exhibited a slight slope, reaching 3.2 mA/cm² at 0.8 V. EIS measured at 35°C, 100% RH, with an anode/cathode gas flow of 1 slpm hydrogen/1 slpm nitrogen at atmospheric pressure, yielded an HFR of 0.145 Ohm*cm². Subsequently, polarization curves and limiting currents were obtained and compared with data from CCMs prepared by ASM.

The CCMs prepared via ASM, using the same catalyst, GDL, and PEM, had the same I/C ratio and a slightly higher catalyst loading (0.372 mgPt/cm²). Compared to the ASM-prepared CCM (Figure 3.9b), the BCM-prepared CCM had similar activation and ohmic polarization losses, but higher mass transport polarization. In the limiting current test, the oxygen transport resistance of the BCM-prepared CCM at 95% RH was 0.117 s/cm, slightly lower than ASM's 0.14 s/cm.

Electrochemical characterization results indicate that BCM is feasible for preparing *Pemion* MEAs, but the current CCM still falls short of performance than CCM fabricated by ASM, especially in the mass transport region. Future research will need to continue adjusting the catalyst ink formulation to achieve better coating effects.

3.3 Limiting Current Test

In this study, the *Nafion* CCM prepared in section 3.1.1 was used to investigate the effects of different scan rates and RH during testing on oxygen transport resistance (OTR). The tests were conducted at 80°C, with an anode/cathode gas flow of 1 slpm hydrogen/4 slpm 1%-5% oxygen/99%-95% nitrogen. Calculation of oxygen transport resistance is carried out by equation 2.2. By plotting backpressure vs. R_t and take the y-intercept of the fitting line (Figure 3.10a), the oxygen transport resistance can be gain. The tests were carried out at scan rates of 5 mV/s and 10 mV/s, yielding consistent results for both the limiting current and OTR. Tests were also performed at 60%, 75%, and 100% RH, revealing that the measured OTR significantly decreased as the RH increased (Figure 3.10b).

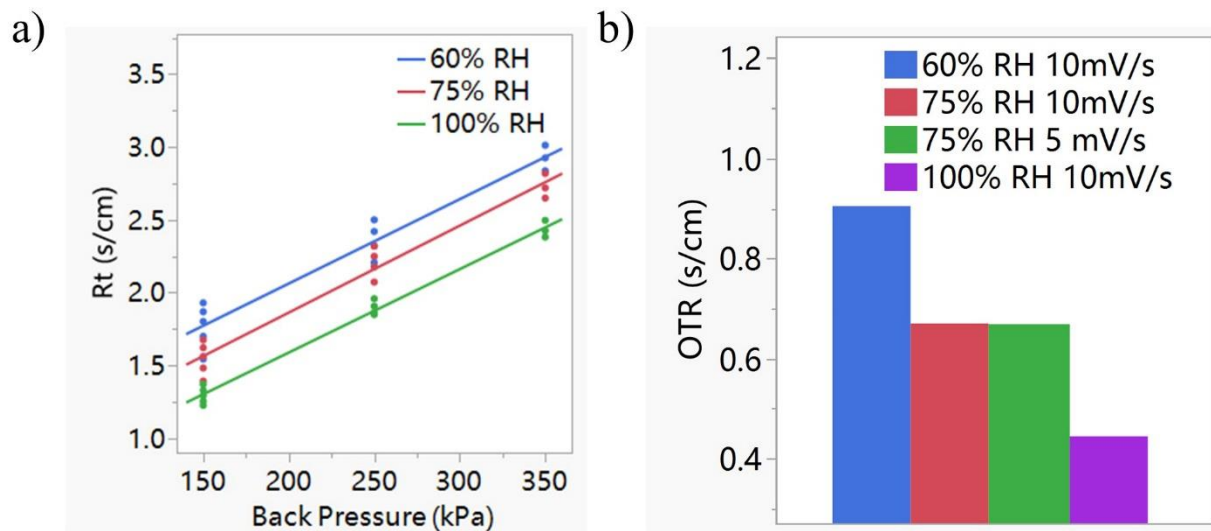


Figure 3.10. Oxygen transport resistance tested under different backpressure and scanning speed.

a) plotting of backpressure vs. R_t , which is calculated in equation 2.2; b) calculated OTR under different condition. The bar plot shows that the OTR would decrease as RH increase, while scanning rate would not have significant influence to the OTR.

3.4 BCM with Other Materials

In addition to the main research activities mentioned above, BCM has been applied to other contexts, but without favorable outcomes.

There was an attempt to prepare a gas diffusion electrode (GDE) on GDL MB30 using BCM, but due to the presence of the PTL, the GDL exhibited excessive absorption of the catalyst ink. Even without the use of a vacuum pump, the catalyst ink was entirely absorbed by the upper half of the GDL and failed to coat the lower half following the blade.

Attempts were made to apply BCM to coat an Fe-N-C catalyst layer on a *Versogen* Piperion membrane. Given the high target loading (4.5 mgC/cm^2), the preparation process itself was not particularly challenging. However, the CCM exhibited bad durability, experiencing failure during the conditioning process.

SUMMARY AND CONCLUSION

In this study, *Pemion*-based CCM was successfully prepared through blade coating method (BCM). The current density at 0.7 V from HFR-corrected polarization curve is 0.8 A/cm², which is same as the CCM fabricated by air-spraying method (ASM).

This study found that by introducing ethylene glycol into the solvent system to alter the viscosity of the catalyst ink, BCM can be used to prepare uniform catalyst layers even at lower target catalyst loadings. By improving the composition of the catalyst ink and the coating method, using *Nafion* NR211 and TKK HSA Carbon Pt/C, a *Nafion* CCM was prepared with an active area of 5 cm², a cathode catalyst loading of 0.26 mgPt/cm², and an I/C ratio of 0.9 via BCM. CO stripping data indicated that the ECSA of this CCM was 52.63 m²/g, aligning with expectations for the TKK HSA carbon Pt/C catalyst used. Compared to CCMs prepared via ASM, this CCM exhibited comparable electrochemical performance and better catalyst layer distribution. Additionally, this research demonstrated that BCM is also suitable for CCMs based on *Pemion* ionomer and provided directions for optimizing the composition of the catalyst ink. Future work will focus on fine-tuning the content of ethylene glycol in the solvent to find the optimal catalyst ink formulation for preparing *Pemion* CCMs. Moreover, future efforts will explore ways to apply BCM on *Pemion* PEMs, ultimately aiming to prepare MEAs free from PFAS components using BCM.

REFERENCE

- [1] International Energy Agency. World Energy Outlook 2021. Int Energy Agency, 2021:15.
- [2] Sherif, S. A., Barbir, F., & Veziroglu, T. N. "Wind energy and the hydrogen economy: review of the technology." *Solar Energy*, vol. 78, pp. 647-660, 2005.
- [3] California Independent System Operator. "Wind and Solar Curtailment." 2020. Available at: https://www.caiso.com/Documents/FlexibleResourcesHelpRenewables_FastFacts.pdf
- [4] Saeedmanesh, A., Mac Kinnon, M. A., & Brouwer, J. "Hydrogen is essential for sustainability." *Current Opinion in Electrochemistry*, vol. 12, pp. 166-181, 2018. <https://doi.org/10.1016/j.coelec.2018.11.009>
- [5] Pascuzzi, S., Anifantis, A., Blanco, I., & Scarascia Mugnozza, G. "Electrolyzer Performance Analysis of an Integrated Hydrogen Power System for Greenhouse Heating: A Case Study." *Sustainability*, vol. 8, 629, 2016.
- [6] Ruth, M. F., Jadun, P., Gilroy, N., Connelly, E., Boardman, R., Simon, A. J., Zuboy, A. E., & J. "The Technical and Economic Potential of the H2@Scale Hydrogen Concept within the United States." 2020:196.
- [7] "Hydrogen Shot: An Introduction." 2022:2362.
- [8] "Table 2-8 Inventory of U.S. Greenhouse Gas Emissions and Sinks, 1990 to 2020." 2020.
- [9] Mazloomi, K., & Gomes, C. "Hydrogen as an energy carrier: Prospects and challenges." *Renewable and Sustainable Energy Reviews*, vol. 16, pp. 3024-3033, 2012.
- [10] Lee, S. A., Jun, S. E., Park, S. H., Kwon, K. C., Kang, J. H., Kwon, M. S., & Jang, H. W. "Single Atom Catalysts for water electrolysis: From catalyst-coated substrate to catalyst-coated membrane." *EES Catalysis*, vol. 2, no. 1, pp. 49–70, 2024. <https://doi.org/10.1039/d3ey00165b>

- [11] Wang, Y., Chen, K. S., Mishler, J., et al. "A review of polymer electrolyte membrane fuel cells: Technology, applications, and needs on fundamental research." *Applied Energy*, vol. 88, no. 4, pp. 981-1007, 2011.
- [12] Yang, D. "Understanding the Formation-Structure-Functionality Relationship of the Catalyst Layer in a Proton Exchange Membrane Fuel Cell."
- [13] Wang, Y., Diaz, D. F. R., Chen, K. S., Wang, Z., & Adroher, X. C. "Materials, technological status, and fundamentals of PEM fuel cells—a review." *Materials Today*, vol. 32, pp. 178-203, 2020.
- [14] Khedekar, K. B. "Understanding Degradation in Polymer Electrolyte Fuel Cells for Light and Heavy-duty Vehicle Applications."
- [15] Harzer, G. S. "Boosting High Current Density Performance of Durable, Low Pt-Loaded PEM Fuel Cells." 2018.
- [16] European Chemicals Agency. "Safety Data Sheet." 2021. Available at: <https://echa.europa.eu/documents/10162/f605d4b5-7c17-7414-8823-b49b9fd43aea>
- [17] Nguen, et al. "Hydrocarbon-based Pemion™ proton exchange membrane fuel cells with state-of-the-art performance." Royal Society of Chemistry, June 2021.
- [18] Kusoglu, & Weber. "Chemical Reviews," vol. 117, pp. 987-1104, 2017.
- [19] Mirfarsi, S. H., Kumar, A., Jeong, J., Adamski, M., McDermid, S., Britton, B., & Kjeang, E. "High-temperature stability of hydrocarbon-based Pemion® Proton Exchange Membranes: A thermo-mechanical stability study." *International Journal of Hydrogen Energy*, vol. 50, pp. 1507–1522, 2024. <https://doi.org/10.1016/j.ijhydene.2023.07.236>

[20] Forner-Cuenca, A. "Novel Gas Diffusion Layers with Patterned Wettability for Advanced Water Management Strategies in Polymer Electrolyte Fuel Cells." 2017.

<https://doi.org/10.3929/ETHZ-A-010811344>

[21] Parkinson, D. Y., Connolly, L. G., & Weber, A. Z. "Gas-diffusion-layer structural properties under compression via X-ray tomography." *Journal of Power Sources*, vol. 328, pp. 364-376, 2016. <https://doi.org/10.1016/j.jpowsour.2016.08.020>

[22] Vinothkannan, M., Kim, A. R., & Yoo, D. J. "Potential carbon nanomaterials as additives for state-of-the-art nafion electrolyte in proton-exchange membrane fuel cells: A concise review." *RSC Advances*, vol. 11, no. 30, pp. 18351-18370, 2021.

<https://doi.org/10.1039/d1ra00685a>

[23] Turtayeva, Z., Xu, F., Dillet, J., Mozet, K., Peignier, R., Celzard, A., & Maranzana, G. "Manufacturing catalyst-coated membranes by ultrasonic spray deposition for PEMFC: Identification of key parameters and their impact on PEMFC performance." *International Journal of Hydrogen Energy*, vol. 47, no. 36, pp. 16165-16178, 2022.

<https://doi.org/10.1016/j.ijhydene.2022.03.043>

[24] Liang, X., Pan, G., Xu, L., & Wang, J. "A modified decal method for preparing the membrane electrode assembly of proton exchange membrane fuel cells." *Fuel*, vol. 139, pp. 393-400, 2015. <https://doi.org/10.1016/j.fuel.2014.09.022>

[25] Zhang, H.; Wang, X.; Zhang, J.; Zhang, J. "Conventional Catalyst Ink, Catalyst Layer and MEA Preparation." In *PEM Fuel Cell Electrocatalysts and Catalyst Layers: Fundamentals and Applications*, edited by J. Zhang, Springer London, London, 2008, pp. 889-916.

- [26] Ramaswamy, N., Gu, W., Kumaraguru, S., & Ziegelbauer, J. "Carbon Support Microstructure Impact on High Current Density Transport Resistances in PEMFC Cathode." *Journal of the Electrochemical Society*, 2019.
- [27] H2Tech. "Ionomer Innovations' Pemion hydrocarbon-based proton exchange membrane exceed industry durability targets."
- [28] Ngo, T. T., Yu, T. L., Lin, H.-L. "Influence of the composition of isopropyl alcohol/water mixture solvents in catalyst ink solutions on proton exchange membrane fuel cell performance." *Journal of Power Sources*, vol. 225, pp. 293-303, 2013.
- [29] Yang, F., Xin, L., Uzunoglu, A., Qiu, Y., Stanciu, L., Ilavsky, J., Li, W., & Xie, J. "Investigation of the Interaction between Nafion Ionomer and Surface Functionalized Carbon Black Using Both Ultrasmall Angle X-ray Scattering and Cryo-TEM." *ACS Applied Materials & Interfaces*, vol. 9, no. 7, pp. 6530-6538, 2017.
- [30] Mashio, T., Ohma, A., & Tokumasu, T. "Molecular Dynamics Study of Ionomer Adsorption at a Carbon Surface in Catalyst Ink." *Electrochimica Acta*, vol. 202, 14-23, 2016.
- [31] Welch, C., Labouriau, A., Hjelm, R., Orler, B., Johnston, C., & Kim, Y. S. "Nafion in Dilute Solvent Systems: Dispersion or Solution?" *ACS Macro Letters*, vol. 1, no. 12, pp. 1403-1407, 2012.
- [32] Baker, D. R., Wieser, C., Neyerlin, K. C., & Murphy, M. W. "The Use of Limiting Current to Determine Transport Resistance in PEM Fuel Cells." *Journal of the Electrochemical Society*, vol. 3, pp. 989-999, 2006. <https://doi.org/10.1149/1.2356218>
- [33] Greszler, T. A., Caulk, D., & Sinha, P. "The Impact of Platinum Loading on Oxygen Transport Resistance." *Journal of the Electrochemical Society*, vol. 159, F831-F840, 2012. <https://doi.org/10.1149/2.061212jes>

- [34] Mayrhofer, K. J. J., Strmcnik, D., Blizanac, B. B., Stamenkovic, V., Arenz, M., & Markovic, N. M. "Measurement of oxygen reduction activities via the rotating disc electrode method: From Pt model surfaces to carbon-supported high surface area catalysts." *Electrochimica Acta*, vol. 53, no. 7, pp. 3181-3188, 2008. <https://doi.org/10.1016/j.electacta.2007.11.057>
- [35] Chanal, D., Yousfi Steiner, N., Petrone, R., Chamagne, D., & Péra, M.-C. "Online diagnosis of PEM fuel cell by fuzzy c-means clustering." *Encyclopedia of Energy Storage*, pp. 359–393, 2022. <https://doi.org/10.1016/b978-0-12-819723-3.00099-8>
- [36] Martin, S., Jensen, J. O., Li, Q., Garcia-Ybarra, P. L., & Castillo, J. L. (2019). "Feasibility of ultra-low Pt loading electrodes for high temperature proton exchange membrane fuel cells based in phosphoric acid-doped membrane." *International Journal of Hydrogen Energy*, vol. 44, no. 52, pp. 28273–28282. <https://doi.org/10.1016/j.ijhydene.2019.09.073>
- [37] Kim, K.-H., Lee, K.-Y., Kim, H.-J., Cho, E., Lee, S.-Y., Lim, T.-H., Yoon, S. P., Hwang, I. C., & Jang, J. H. (2010). "The effects of Nafion® ionomer content in PEMFC MEAs prepared by a catalyst-coated membrane (CCM) spraying method." *International Journal of Hydrogen Energy*, vol. 35, no. 5, pp. 2119–2126. <https://doi.org/10.1016/j.ijhydene.2009.11.058>
- [38] Deschamps, F. L., Mahy, J. G., Léonard, A. F., Lambert, S. D., Dewandre, A., Scheid, B., & Job, N. (2020). "A practical method to characterize proton exchange membrane fuel cell catalyst layer topography: Application to two coating techniques and two carbon supports." *Thin Solid Films*, vol. 695, 137751. <https://doi.org/10.1016/j.tsf.2019.137751>
- [39] Liang, X., Pan, G., Xu, L., & Wang, J. (2015). "A modified decal method for preparing the membrane electrode assembly of proton exchange membrane fuel cells." *Fuel*, vol. 139, pp. 393–400. <https://doi.org/10.1016/j.fuel.2014.09.022>

[40] Mehmood, A., & Ha, H. Y. (2012). "An efficient decal transfer method using a roll-press to fabricate membrane electrode assemblies for direct methanol fuel cells." *International Journal of Hydrogen Energy*, vol. 37, no. 23, pp. 18463–18470.

<https://doi.org/10.1016/j.ijhydene.2012.09.045>

[41] Cho, H. J., Jang, H., Lim, S., Cho, E., Lim, T.-H., Oh, I.-H., Kim, H.-J., & Jang, J. H. (2011). "Development of a novel decal transfer process for fabrication of high-performance and reliable membrane electrode assemblies for PEMFCs." *International Journal of Hydrogen Energy*, vol. 36, no. 19, pp. 12465–12473. <https://doi.org/10.1016/j.ijhydene.2011.06.113>

[42] Shahgaldi, S., Alaefour, I., Unsworth, G., & Li, X. (2017). "Development of a low temperature decal transfer method for the fabrication of proton exchange membrane fuel cells." *International Journal of Hydrogen Energy*, vol. 42, no. 16, pp. 11813–11822.

<https://doi.org/10.1016/j.ijhydene.2017.02.127>

[43] Liu, G., Peng, S., Hou, F., Wang, X., & Fang, B. (2022). "Preparation and performance study of the Anodic Catalyst Layer via doctor blade coating for PEM water electrolysis." *Membranes*, vol. 13, no. 1, 24. <https://doi.org/10.3390/membranes13010024>

[44] Park, I.-S., Li, W., & Manthiram, A. (2010). "Fabrication of catalyst-coated membrane-electrode assemblies by doctor Blade Method and their performance in Fuel Cells." *Journal of Power Sources*, vol. 195, no. 20, pp. 7078–7082. <https://doi.org/10.1016/j.jpowsour.2010.05.004>

[45] Hsu, C. (2003). "An innovative process for PEMFC electrodes using the expansion of Nafion Film." *Journal of Power Sources*, vol. 115, no. 2, pp. 268–273.

[https://doi.org/10.1016/s0378-7753\(03\)00005-3](https://doi.org/10.1016/s0378-7753(03)00005-3)

[46] Huang, D.-C., Yu, P.-J., Liu, F.-J., Huang, S.-L., Hsueh, K.-L., Chen, Y.-C., Wu, C.-H., Chang, W.-C., & Tsau, F.-H. (2011). "Effect of dispersion solvent in catalyst ink on proton

exchange membrane fuel cell performance." *International Journal of Electrochemical Science*, vol. 6, no. 7, pp. 2551–2565. [https://doi.org/10.1016/s1452-3981\(23\)18202-2](https://doi.org/10.1016/s1452-3981(23)18202-2)